

Chapter 1

Parton energy loss and momentum broadening at NLO in high temperature QCD plasmas

Jacopo Ghiglieri

*Institute for Theoretical Physics, Albert Einstein Center,
University of Bern, Sidlerstrasse 5, 3012 Bern, Switzerland
jacopo.ghiglieri@itp.unibe.ch*

Derek Teaney

*Department of Physics and Astronomy, Stony Brook University,
Stony Brook, New York 11794-3800, United States
derek.teaney@stonybrook.edu*

We present an overview of a perturbative-kinetic approach to jet propagation, energy loss, and momentum broadening in a high temperature quark-gluon plasma. The leading-order kinetic equations describe the interactions between energetic jet-particles and a non-abelian plasma, consisting of on-shell thermal excitations and soft gluonic fields. These interactions include $2 \leftrightarrow 2$ scatterings, collinear bremsstrahlung, and drag and momentum diffusion. We show how the contribution from the soft gluonic fields can be factorized into a set of Wilson line correlators on the light cone. We review recent field-theoretical developments, rooted in the causal properties of these correlators, which simplify the calculation of the appropriate Wilson lines in thermal field theory. With these simplifications lattice measurements of transverse momentum broadening have become possible, and the kinetic equations describing parton transport have been extended to next-to-leading order in the coupling g .

1. Introduction

The suppression of highly energetic jets (or jet quenching) is one of the most striking findings of the experimental program of heavy-ion collisions.^{1–5} A comprehensive review⁶ can be found in this volume, which also contains another contribution reviewing a specific approach in greater detail.⁷

In this review, we concentrate on a weakly-coupled kinetic approach describing the propagation of high momentum jet-like particles through a Quark-Gluon Plasma (QGP). A detailed perturbative description of the QGP and jet-quenching is available when the temperature is high $T \gg \Lambda_{QCD}$, and the momentum of the jet-particles is much larger than the temperature, $p \gg T$.

The kinetic picture of the high temperature QGP, which has emerged through a combination of physical intuition, direct diagrammatic analysis, and a gradient expansion, is characterized by hard particles and random classical non-abelian fields.^{8–11} We will describe a Boltzmann equation for the propagation of jet-like particles interacting with the hard particles and random fields which comprise this idealized weakly coupled plasma. Here the jet-particles have momentum $p \gg T$, while the hard particles have momentum $\sim T$, and the random classical fields are soft with momenta of order gT , $p \gg T \gg gT$, where g is the strong coupling constant. For simplicity, we will limit the discussion to pure gauge theory. As discussed in Section 2, to leading order in the coupling constant there are three processes relevant to the transport of jet-particles in the high temperature plasma: (i) $2 \leftrightarrow 2$ elastic scatterings with hard particles, (ii) collinear radiation, and (iii) drag and momentum diffusion driven by the soft classical background.

The interactions between the jet-particles and the classical non-abelian fields, requires a resummation scheme known as the Hard Thermal Loop (HTL) effective theory,^{8,9} which is the QCD analog of the Vlasov equations.¹⁰ This effective theory is necessary to compute the drag coefficients and collinear bremsstrahlung rates which describe the propagation of jets. The computational complexity of the Vlasov equations would, at first sight, make any extension beyond leading order in the coupling extremely challenging. However, Hard Thermal Loops correlators (and statistical correlators more generally) simplify greatly when evaluated at lightlike separations.¹² It is precisely such light-like correlators which must be evaluated to determine the drag, diffusion, and collinear bremsstrahlung rates of jet-particles propagating in plasma.

These simplifications are a consequence of the following physical picture: Since the hard and jet-particles are propagating almost exactly along the light cone, they are probing an essentially undisturbed plasma, at least as far as the soft classical background is concerned. Informally, we say that the soft classical background “can’t keep up” with the hard or jet-particle traversing the plasma. Thus, the soft correlations that are probed by the hard and jet-particles are statistical in nature rather than dynamical.

In Sec. 3 we will illustrate the basics of Hard Thermal Loops and then proceed to introduce the field-theoretical arguments for the light-like simplifications, originally due to Caron-Huot.¹² We then use these simplifications at leading order to determine the transverse momentum diffusion and drag coefficients for high momentum probes.

An important consequence of these lightlike simplifications and their physical origin (see above) is that lattice techniques can be used to compute several lightlike correlators, which arise in jet-quenching physics. Due to the Minkowskian nature of the problem and the large energies at play, a direct ab-initio lattice calculation of jet propagation in medium is not feasible. However, as we show in detail, the soft contribution to quantities such as \hat{q} (the jet quenching parameter) becomes

Euclidean and three-dimensional, which makes it amenable to lattice measurements. In Sec. 4 we illustrate the basic principles of the dimensionally reduced (three-dimensional) effective theory, and review the first lattice calculation¹³ of the soft contribution to \hat{q} .

Of course, the special properties of HTLs on the lightcone also simplify perturbative calculations. Indeed, Caron-Huot employed these results to compute \hat{q} and the transverse scattering kernel to NLO¹² in the strong coupling constant g . Building on this and related developments, the photon and low-mass dilepton emission rates were also computed to NLO.^{14,15} These electromagnetic rates at NLO correct the strictly collinear approximations made at leading order. Finally, this review anticipates an upcoming publication by the current authors where the LO Boltzmann equation for jet-transport described above is extended to NLO.¹⁶ In Sect. 5 we sketch the Boltzmann equation to this order, which includes the drag coefficient at NLO and semi-collinear emission rates describing bremsstrahlung at wider angles. Many of the parameters of the effective kinetic theory, such as drag coefficients, thermal masses, and the transverse collision kernel, can be computed using the three-dimensional lattice described above, providing a tantalizing semi-perturbative description of energy loss. These results and future directions are summarized in Sec. 6.

2. The kinetic picture at leading order

In this section we will summarize the kinetics of high temperature weakly coupled non-abelian plasmas. As we mentioned in the introduction, this kinetic picture of the QGP is characterized by hard particles and random classical non-abelian fields.⁸⁻¹¹ First we will describe the interactions between these constituents qualitatively, and subsequently give a more quantitative description. We are particularly interested in formulating a Boltzmann equation for the transport of high momentum gluons $p \gg T$ traversing the QGP, *i.e.* a Boltzmann equation for jet-particles interacting with the hard particles and random classical fields which comprise the high temperature plasma. The phase space distribution of the jet-particles is notated with $f(t, \mathbf{x}, \mathbf{p})$ (or $f_{\mathbf{p}}$ when clear from context) while the phase space distribution of the equilibrium hard particles is notated with $n(t, \mathbf{x}, \mathbf{p})$ (or $n_{\mathbf{p}}$).

The interactions between the particles and the classical fields of the QGP are characterized by three processes:

- (1) First, there are $2 \leftrightarrow 2$ collisions between the hard and the jet-particles. These scattering events are strongly localized in space-time.
- (2) Second, the random classical fields in the plasma induce drag and momentum diffusion and change the momenta of the jet-particles in characteristic ways. The drag and diffusion coefficients are calculated by examining the response of the classical fields to the non-equilibrium jet-particle.
- (3) Finally, the momentum diffusion produced by the random classical field induces

collinear bremsstrahlung, causing the jet-particles to split collinearly.

At leading order in the coupling g , the Boltzmann equation for the jet-particles takes the form

$$\left(\frac{\partial}{\partial t} + \mathbf{v}_{\mathbf{p}} \cdot \frac{\partial}{\partial \mathbf{x}} \right) f(t, \mathbf{x}, \mathbf{p}) = C_{2 \leftrightarrow 2}[\mu] + C_{\text{diff}}[\mu] + C_{\text{coll}}, \quad (1)$$

where the three rates on the right-hand-side reflect these three processes. We have anticipated that the $2 \leftrightarrow 2$ and diffusion rates depend on a separation scale μ , but the dependence on μ cancels when both processes are included. In the remainder of this section we will discuss each of these rates in greater detail.

The hard particles are approximately on-shell and carry the majority of the energy and momentum of the plasma. For this reason these hard constituents are the most important for the thermodynamics of the QGP, and the soft fields are only important insofar as they influence the kinetics of the jet and hard particles. The typical momentum of these excitations is of order the temperature, but the virtuality is of order $\sim g^2 T^2$. Specifically, for a hard particle moving in the positive z direction, the scaling of momentum in lightcone coordinates is^a

$$P^\mu = (p^+, p^-, \mathbf{p}_\perp), \quad (3)$$

$$= (T, g^2 T, gT). \quad (4)$$

Squaring this momentum shows that the virtuality of these on shell constituents is of order $P^2 \sim g^2 T^2$. To estimate the contribution of these on-shell constituents to the plasma energy density we use the equilibrium distribution function, $n_{\mathbf{p}} = 1/(e^{E_{\mathbf{p}}/T} - 1)$, and write

$$e(t, \mathbf{x}) = 2d_A \int_{\sim gT}^{\infty} \frac{d^3 p}{(2\pi)^3} E_{\mathbf{p}} n_{\mathbf{p}}. \quad (5)$$

First, we note that the integral is cut off when the three-momentum of the constituents is soft, $p \sim gT$. At this point the power counting implicit in Eq. (3) no longer applies. Taking the free gas dispersion relation $\epsilon_{\mathbf{p}} = p$, we see that the contribution of the soft modes ($p \lesssim gT$) is of order $g^3 T^4$, while the leading contribution is of order T^4 .

The first correction to the free gas result for thermodynamic properties the QGP can be found by determining the correction to the dispersion curve for the on-shell particles. Specifically, the dispersion curve (the relation between $E_{\mathbf{p}}$ and \mathbf{p}) is found by evaluating the one-loop self energy for an approximately on shell gluon. The self-energy diagram involves internal lines of momentum

$$Q^\mu = (q^+, q^-, q_\perp) \sim (T, T, T), \quad (6)$$

^a We use a notation where $p^+ = \frac{p^0 + p^z}{2}$, $p^- = p^0 - p^z$, four-vectors are denoted by uppercase letters and the metric is the “mostly-plus” one, so that $P^2 = -2p^+ p^- + p_\perp^2$. The integration measure is

$$\int \frac{d^4 P}{(2\pi)^4} = \int \frac{dp_+ dp_- d^2 p_\perp}{(2\pi)^4}. \quad (2)$$

and are thus highly virtual compared to the on-shell particles. The effect of these virtual modes (which are integrated out in any kinetic description) is to change the dispersion relation of the on-shell modes

$$E_{\mathbf{p}} = p + \frac{m_{\infty}^2}{2p} + \dots, \quad (7)$$

where the ellipses indicate higher order corrections. Here we have defined the leading order gluon asymptotic mass in pure gauge theory at high temperature^{17–20}

$$m_{\infty}^2 = 2g^2 C_A \int \frac{d^3 p}{(2\pi)^3} \frac{n_B}{p} = \frac{1}{6} g^2 C_A T^2. \quad (8)$$

As discussed in Sec. 5, the asymptotic mass can be expressed as a correlator of field strengths along the light cone, which is closely related to an analogous correlator for \hat{q} , see Eq. (80).

These hard modes with $p \sim T$ occasionally collide with the jet partons, transferring momenta of order the temperature. At leading order these collisional processes are $2 \leftrightarrow 2$ processes, which can be localized in space-time to within a distance of $\sim 1/T$. A kinetic equation for the phase space distribution function of the jet partons including such scattering processes takes the form

$$\left(\frac{\partial}{\partial t} + \mathbf{v}_{\mathbf{p}} \cdot \frac{\partial}{\partial \mathbf{x}} \right) f_{\mathbf{p}}(t, \mathbf{x}) = C_{2 \leftrightarrow 2}[\mu] + \dots, \quad (9)$$

where the ellipses will be described below. The velocity in this equation is the group velocity, $\mathbf{v}_{\mathbf{p}} = \partial E_{\mathbf{p}} / \partial \mathbf{p}$. The collision rate between the hard modes and the jet particles takes the form^b

$$\begin{aligned} -C_{2 \leftrightarrow 2}[\mu] = & \frac{1}{4d_A} \int_{\mathbf{p}' \mathbf{k} \mathbf{k}'} \frac{|\mathcal{M}|^2}{(2p)(2p')(2k)(2k')} (2\pi)^4 \delta^4(P + P' - K - K') \\ & \times \left[f_{\mathbf{p}} n_{\mathbf{p}'} (1+n_{\mathbf{k}})(1+n_{\mathbf{k}'}) - f_{\mathbf{k}} n_{\mathbf{k}'} (1+n_{\mathbf{p}}) - n_{\mathbf{k}} f_{\mathbf{k}'} (1+n_{\mathbf{p}'}) \right], \end{aligned} \quad (10)$$

where in the second line we have dropped terms that are exponentially suppressed for $p \gg T$.^c The kinematics of the collisional process with momentum exchange of order $\sim T$ is shown in fig. 1. The squared matrix element (summed over initial and final state colors and helicities) may be obtained from vacuum perturbation theory:

$$|\mathcal{M}|^2 = 16d_A g^4 C_A^2 \left(3 - \frac{su}{t^2} - \frac{st}{u^2} - \frac{tu}{s^2} \right). \quad (11)$$

The $2 \leftrightarrow 2$ scattering rate is divergent in the infrared, and therefore we have notated the dependence on the separation scale μ in Eq. (10). There are many

^bWe use a familiar shorthand notation, $\int_{\mathbf{p} \mathbf{k} \mathbf{k}'} \equiv \int \frac{d^3 p}{(2\pi)^3} \frac{d^3 k}{(2\pi)^3} \frac{d^3 k'}{(2\pi)^3}$, and we are neglecting the thermal mass when writing Eq. (10). The leading factor of $1/(4d_A)$ reflects an average over spins and colors of the external gluon and a symmetry factor $1/2$ for the sum over final states.

^cWe consider $\exp(-p/T) \ll 1$. In the remainder of this review we sometimes treat T/P as an explicit expansion parameter for illustration purposes. The detailed exposition and the calculations in¹⁶ are performed without treating T/P as an expansion parameter.

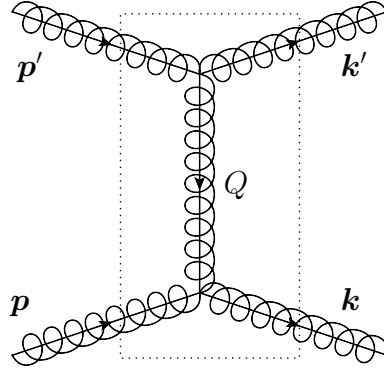


Fig. 1. Hard $2 \leftrightarrow 2$ collision contributing the collision rate $C_{2 \leftrightarrow 2}[\mu]$. Only hard lines which enter or exit the boxed region are included in an effective Boltzmann description.

ways this divergence can be regulated. At leading and next-to-leading we find it convenient¹⁶ to simply cutoff the transverse momentum exchange at small q_\perp , $q_\perp > \mu$. It is not difficult to extract the logarithmic dependence on μ for $\mu \ll T$. Indeed, let us consider for illustration a leading-log approximation to $C_{2 \leftrightarrow 2}[\mu]$: we expand the distribution function and matrix elements to second order in the exchange momentum Q and arrive at a Fokker-Planck equation^{21–23} for $f_{\mathbf{p}}$

$$C_{2 \leftrightarrow 2}[\mu] = \hat{e}_{UV}(\mu) v^i \frac{\partial f_{\mathbf{p}}}{\partial p^i} + \frac{1}{2} \hat{q}_{UV}^{ij}(\mu) \frac{\partial^2 f_{\mathbf{p}}}{\partial p^i \partial p^j} + \mathcal{O}\left(\frac{T}{p}\right) + \mu\text{-independent}, \quad (12)$$

In writing this equation we have dropped terms suppressed by T/p . Here \hat{v} is a unit vector in the direction of \mathbf{p} , and the diffusion tensor $\hat{q}_{UV}^{ij}(\mu)$ controls the longitudinal and transverse momentum diffusion,

$$\hat{q}_{UV}^{ij}(\mu) \equiv \hat{q}_{L,UV}(\mu) \hat{v}^i \hat{v}^j + \frac{1}{2} \hat{q}_{UV}(\mu) (\delta^{ij} - \hat{v}^i \hat{v}^j). \quad (13)$$

The values of these coefficients are found from the expansion of Eq. (10), and for pure gauge are at leading log

$$\hat{q}_{UV}(\mu) = g^2 C_A T \frac{m_D^2}{2\pi} \log\left(\frac{T}{\mu}\right), \quad (14)$$

$$\hat{q}_{L,UV}(\mu) = g^2 C_A T \frac{m_\infty^2}{2\pi} \log\left(\frac{T}{\mu}\right). \quad (15)$$

Here the Debye mass is given by the integral over distribution functions

$$m_D^2 = 2g^2 C_A \int \frac{d^3 p}{(2\pi)^3} \frac{n_p(1+n_p)}{T} = \frac{1}{3} g^2 C_A T^2, \quad (16)$$

and the asymptotic mass is given by a similar integral in Eq. (8). At this point the interpretation of these thermodynamic integrals as the Debye and asymptotic masses is premature. This interpretation will be clear from Sec. 3, which explains

physically why the transverse diffusion coefficient involves the Debye mass, while the longitudinal diffusion involves the asymptotic mass.

The fluctuation-dissipation theorem relates the coefficient of $\hat{q}_{L,UV}(\mu)$ to $\hat{e}_{UV}(\mu)$

$$q_{L,UV}(\mu) = 2T\hat{e}_{UV}(\mu) + \mathcal{O}\left(\frac{T}{p}\right). \quad (17)$$

This Einstein relation is necessary in order for $f_{\mathbf{p}}$ to reach its equilibrium form $e^{-p/T}$ under the Fokker-Planck evolution in Eq. (12). Since the equilibrium distribution is a stationary solution to the full $2 \leftrightarrow 2$ Boltzmann equation (Eq. (10)) this relation between the drag and the longitudinal diffusion coefficient automatically arises from a direct expansion of the Boltzmann equation.^{16,24,25}

As we will see, the cutoff dependence in the $2 \leftrightarrow 2$ contribution to the Boltzmann equation cancels when the interactions with the soft background fields are included. The description of these soft modes is our next task. As discussed above, the virtuality of the hard modes is of order $P^2 \sim (gT)^2$ with the momentum scaling given in Eq. (3). The soft gluonic excitations, on the other hand, have a momentum scaling

$$P^\mu = (gT, gT, gT), \quad (18)$$

but also have virtuality of order $P^2 \sim (gT)^2$. Since these modes are soft, they are highly occupied due to the Bose-Einstein distribution function

$$n_B(p^0) \simeq \frac{T}{p^0} \sim \frac{1}{g}. \quad (19)$$

Thus, at leading order these soft modes can be treated as a classical gluonic field interacting with the hard on-shell modes.

It is important to emphasize that the energy in these soft modes constitutes a small fraction of the total energy density. Nevertheless, they significantly influence the kinetics of the on-shell particles. Specifically, these soft modes collide frequently with the hard and jet particles and exchange soft momenta of order gT . It seems intuitive that the effect of these soft scatterings can be incorporated into a Fokker-Planck equation describing the drag and momentum diffusion of the jet (and hard) particles

$$\left(\partial_t + v_{\mathbf{p}} \cdot \frac{\partial}{\partial \mathbf{x}}\right) f_{\mathbf{p}} = C_{\text{diff}}[\mu] + \dots, \quad (20)$$

The collision (or Fokker-Planck) operator can be written as

$$C_{\text{diff}}[\mu] = \hat{e}(\mu) v^i \frac{\partial f}{\partial p^i} + \frac{1}{2} \hat{q}^{ij}(\mu) \frac{\partial^2 f}{\partial p^i \partial p^j} + \mathcal{O}\left(\frac{T}{P}\right), \quad (21)$$

where the momentum diffusion parallel and perpendicular to the direction of motion \mathbf{p} are quantified by $\hat{q}^{ij}(\mu)$ and the fluctuation-dissipation theorem is satisfied as

described above^d. Terms of higher order in T/p are discussed in detail elsewhere.¹⁶

We have emphasized that the parameters of the Fokker-Planck evolution depend on the scale μ separating the scattering from soft modes, and the scattering from hard $2 \leftrightarrow 2$ collisions. As the separation scale is changed, the parameters of the Fokker-Planck equation change and the drag and diffusion rates change accordingly. Indeed, Sec. 3 shows that at leading order the drag and diffusion coefficients are

$$\hat{q}(\mu) = g^2 C_A T \frac{m_D^2}{2\pi} \log \left(\frac{\mu}{m_D} \right), \quad (22a)$$

$$\hat{q}_L(\mu) = g^2 C_A T \frac{m_\infty^2}{2\pi} \log \left(\frac{\mu}{m_\infty} \right). \quad (22b)$$

Thus, a change in these coefficients due to a change in μ is compensated by a corresponding change in the hard $2 \leftrightarrow 2$ collision operator in Eq. (12).

As is well known the Fokker-Planck evolution specified by Eq. (21) is equivalent to a Langevin process,²⁷ where each particle in the phase space follows an equation of motion specified by a drag and a stochastic force ξ^i , whose variance is specified by the diffusion coefficients

$$\frac{dp^i}{dt} = -\hat{e}(\mu)v^i + \xi^i, \quad \langle \xi^i(t)\xi^j(t') \rangle = \hat{q}^{ij}(\mu)\delta(t-t'). \quad (23)$$

The Langevin description is valid on timescales which are long compared to the underlying correlation times between the microscopic forces in the medium. For a classical particle satisfying Newton's Law, $dp^i/dt = \mathcal{F}^i$, one would adjust the diffusion coefficient so that the integrated squared variance between the microscopic and stochastic forces agree

$$\hat{q}^{ij}\mathcal{T} \equiv \int dt \int dt' \langle \xi^i(t)\xi^j(t') \rangle = \int dt \int dt' \langle \mathcal{F}^i(t)\mathcal{F}^j(t') \rangle. \quad (24)$$

Here \mathcal{T} is the total time, and the forces are to be evaluated along the trajectory of the particle, *i.e.* for a particle traveling at the speed of light along the z -axis the coordinates are $x^\mu = (x^+, x^-, \mathbf{x}_\perp) = (t, 0, \mathbf{0}_\perp)$. For a hard particle in representation R interacting with a soft classical background QCD field, the forces are $gT_R^a F_a^{i\mu}(x^+)v_\mu$ and are dressed with Wilson lines following the trajectory of the particle along the light cone from past infinity^e

$$\mathcal{F}^i(x^+) \equiv U_R^\dagger(x^+, -\infty) gF^{i\mu}(x^+)v_\mu U_R(x^+, -\infty). \quad (25)$$

^dIn the remainder of this review \hat{q} describes only the contribution of soft gT to transverse momentum broadening, and perhaps should be written as \hat{q}_{soft} . In most of the literature on jet energy loss (see for example ²⁶) \hat{q} refers to the sum of the soft and hard contribution, with a logarithmic sensitivity on the jet energy p .

^eHere and below we use a matrix notation $F^{\mu\nu} = F_a^{\mu\nu} T_R^a$. v^μ is a lightlike four vector $v^\mu = (1, \mathbf{v})$ in the direction of motion of the particle, which is conventionally taken to be along the z axis. Thus, $F^{\mu\nu}v_\mu = F^{i-}$ and note that $F^{z-} = F^{+-}$. More explicitly, the Wilson lines are $U(x^+, 0) = P e^{-i \int_0^{x^+} dx^+ A^-}$.

The appropriate formulas for \hat{q} and q_L are then

$$\hat{q}(\mu) = \frac{1}{d_R} \int_{-\infty}^{\infty} dx^+ \text{Tr} \langle \mathcal{F}_{\perp}(x^+) \mathcal{F}_{\perp}(0) \rangle, \quad (26)$$

$$\hat{q}_L(\mu) = \frac{1}{d_R} \int_{-\infty}^{\infty} dx^+ \text{Tr} \langle \mathcal{F}^z(x^+) \mathcal{F}^z(0) \rangle, \quad (27)$$

where the two transverse directions are summed over in Eq. (26), and the trace averages over the colors of the incoming particle. For a classical background field these correlators can also be written as^f

$$\hat{q}(\mu) = \frac{g^2 C_R}{d_A} \int_{-\infty}^{\infty} dx^+ \langle v_{\mu} F_a^{\mu\nu}(x^+) U_A^{ab}(x^+, 0) v_{\rho} F_{\nu,b}^{\rho}(0) \rangle, \quad (29)$$

$$\hat{q}_L(\mu) = \frac{g^2 C_R}{d_A} \int_{-\infty}^{\infty} dx^+ \langle v_{\mu} F_a^{\mu+}(x^+) U_A^{ab}(x^+, 0) v_{\rho} F_b^{\rho+}(0) \rangle, \quad (30)$$

where $U_A^{ab}(x^+, 0)$ is the adjoint Wilson line.

The evaluation of the transport parameters $\hat{q}_L(\mu)$ and $\hat{q}(\mu)$ using these correlators involves understanding how the hard particles interact with the classical gluon fields at leading and next-to-leading order. This had been carefully examined by Blaizot and Iancu who worked in a background field gauge and systematically employed a gradient expansion to determine the appropriate kinetic equations which are the non-abelian generalization of the Vlasov equations.¹⁰ We will write the non-abelian Vlasov equations in the next section and exhibit the appropriate HTL diagrammatic rules for evaluating these soft classical gluon correlators. Then in Sec. 3 we will show how these rules can be used to arrive at Eq. (22).

The random classical gluonic fields cause the hard and jet particles to diffuse in momentum. This random walk induces collinear bremsstrahlung in medium. We will follow the AMY formalism for computing the collinear bremsstrahlung rate,¹¹ and refer to ref.²⁸ which compares the AMY formalism to other approaches, which are described in the reviews.^{3,5} Collinear bremsstrahlung can be included into the Boltzmann equation and takes the form of a local rate C_{coll} for a hard (approximately massless) gluon to branch into two hard gluons moving in approximately the same direction as their parent²⁹⁻³¹

$$(\partial_t + v_{\mathbf{p}} \cdot \partial_{\mathbf{x}}) f_{\mathbf{p}} = C_{\text{coll}} + \dots \quad (31)$$

To describe the gluon bremsstrahlung rate we refer to fig. 2 which schematically illustrates the collinear radiation induced by the soft scatterings. The kinematics are shown for a gluon with momentum $p = |\mathbf{p}|$ in the longitudinal direction to branch into two gluons moving in approximately the same direction with longitudinal momentum ω and $p - \omega$. Although the bremsstrahlung rate enters the Boltzmann

^f To see this, take $dx^+ = \Delta x^+$ small. Then, evaluate the following trace to first order in Δx^+ to see the structure of the adjoint Wilson line emerge

$$\text{Tr}[\mathcal{F}^z(x^+) \mathcal{F}^z(0)] \simeq v_{\mu} F_a^{z\mu}(x^+) v_{\rho} F_b^{z\rho}(0) \text{Tr}[(1 + ig\Delta x^+ A^-) T^a (1 - ig\Delta x^+ A^-) T^b]. \quad (28)$$

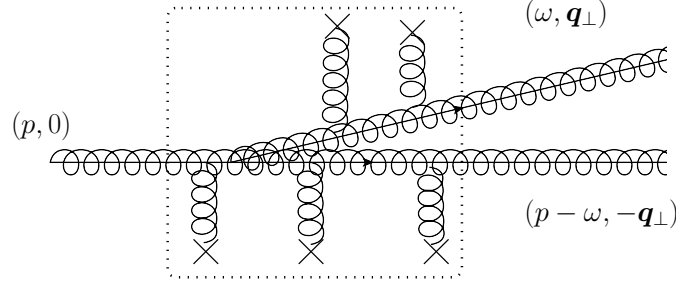


Fig. 2. Schematic Feynman diagram contributing to the leading order collinear bremsstrahlung rate. Hard gluon lines are labeled by their three momentum (p_z, \mathbf{p}_\perp) . The interactions with the random classical background bath are illustrated by the gluon lines with crosses. Only hard lines which enter or exit the boxed region are included in an effective Boltzmann description.

equation as a local rate, it must be understood that the emission process can only be localized to within a time scale set by the formation time of the radiation. The inverse formation time will be defined as the energy difference between the initial and final states

$$(\tau_{\text{form}})^{-1} \equiv \delta E(h, p, \omega) = (E_\omega + E_{p-\omega}) - E_p. \quad (32)$$

Using the dispersion relation for the hard particles this reads

$$\delta E(h, p, \omega) \simeq \frac{h^2}{2p\omega(p-\omega)} + \frac{m_{\infty\omega}^2}{2\omega} + \frac{m_{\infty p-\omega}^2}{2(p-\omega)} - \frac{m_{\infty p}^2}{2p}, \quad (33)$$

where $m_{\infty p}^2$ is the asymptotic mass of the particle with momentum p , as summarized in Eq. (8). We have further defined

$$\mathbf{h} \equiv p\mathbf{q}_\perp. \quad (34)$$

As seen from the figure and described below, \mathbf{h}/p is a transverse momentum vector which is conjugate to the (transverse) coordinate separation \mathbf{x}_\perp between the initial and final states.

The bremsstrahlung rate C_{coll} is determined by the rate of transverse momentum kicks (of magnitude q_\perp) which a hard particle experiences traversing the soft classical fields:

$$C_R(q_\perp) \equiv \lim_{p \rightarrow \infty} (2\pi)^2 \frac{d\Gamma_R(\mathbf{p}, \mathbf{p} + \mathbf{q}_\perp)}{d^2 q_\perp}. \quad (35)$$

Here \mathbf{p} is the momentum of the hard particle, which is large ($\mathbf{p} \rightarrow \infty$) relative to the typical momentum, $\sim gT$, of the background fields. The collision kernel C_R can be expressed as a Wilson loop in the (x^+, x_\perp) plane evaluated in the classical background,^{12,32,33} as sketched in Fig. 3. To motivate the appropriate Wilson loop we note that the average squared momentum transfer per unit time (*i.e.* \hat{q}) is

determined by $\mathcal{C}_R(q_\perp)$

$$\hat{q}(\mu) = \int^\mu \frac{d^2 q_\perp}{(2\pi)^2} q_\perp^2 \mathcal{C}_R(q_\perp). \quad (36)$$

As described above \hat{q} can be expressed as a correlation of field strengths (see Eq. (26)). Numerically at least, this correlation function should be understood as the limit of a Wilson loop (see fig. 3) as the transverse separation approaches zero and the length approaches infinity

$$\lim_{x_\perp \rightarrow 0} \lim_{L \rightarrow \infty} \langle W_R(x_\perp, L) \rangle = \exp \left(-\frac{1}{4} \hat{q}(\mu) x_\perp^2 L \right) \quad (37)$$

It is not difficult to show that this Wilson loop expression agrees with Eq. (26)

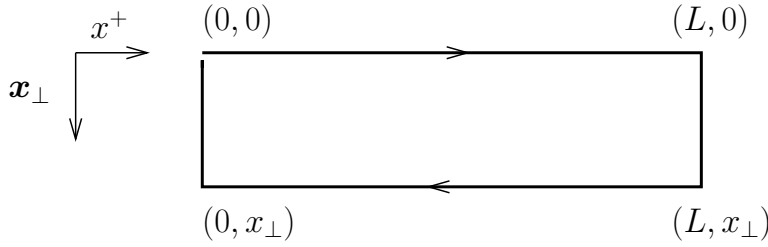


Fig. 3. Wilson loop leading to $\hat{q}(\mu)$. Here the side rails, $P e^{-i \int_0^L dx^+ A^-(x^+, 0)}$ and $P e^{-i \int_L^0 dx^+ A^-(x^+, x_\perp)}$, are separated by transverse coordinates \mathbf{x}_\perp and extend in $x^+ = (t+z)/2$ from $x^+ = 0$ up to $x^+ = L$. x^- is zero in this figure. The Wilson loop is traced over colors, $\frac{1}{d_R} \text{Tr} \dots$, as indicated by the gap at the top left corner.

in the limit of small separation. Although it is not entirely obvious, it is certainly not surprising that the Wilson loop is sufficient to completely determine $\mathcal{C}_R(\mathbf{q}_\perp)$. Specifically, the impact parameter representation of the collision kernel

$$\mathcal{C}_R(x_\perp) = \int \frac{d^2 q_\perp}{(2\pi)^2} (1 - e^{i\mathbf{q} \cdot \mathbf{x}_\perp}) \mathcal{C}_R(\mathbf{q}_\perp), \quad (38)$$

is determined by the asymptotic behavior of the same Wilson loop at large L

$$\lim_{L \rightarrow \infty} \langle W_R(x_\perp, L) \rangle = \exp(-\mathcal{C}_R(\mathbf{x}_\perp) L). \quad (39)$$

Expressions of this form have been used to compute $\hat{q}(\mu)$ at leading and next-to-leading order.

We have described the collision kernel in detail, since it is a key parameter in determining the collinear bremsstrahlung rate. A derivation of this rate is beyond the scope of this review, and here we will simply quote the relevant formulas and describe the relevant physics. The radiation rate for a gluon of momentum p to radiate a gluon of longitudinal momentum ω in approximately the same direction

is^{5,31}

$$\begin{aligned} \left. \frac{d\Gamma(p, \omega)}{d\omega} \right|_{\text{coll}} &= \frac{g^2 C_A}{16\pi p^7} (1 + n(\omega))(1 + n(p - \omega)) \frac{1 + x^4 + (1 - x)^4}{x^3(1 - x)^3} \\ &\times \int \frac{d^2 h}{(2\pi)^2} 2\mathbf{h} \cdot \text{Re } \mathbf{F}(\mathbf{h}, p, \omega), \end{aligned} \quad (40)$$

where $x \equiv \omega/p$ is the longitudinal momentum fraction of one of the outgoing gluons. The leading factor $(1 + x^4 + (1 - x)^4)/(x^3(1 - x)^3)$ records the collinear emission probability accompanying a scattering process. Similarly $\mathbf{F}(\mathbf{h}, p, \omega)$ records the time evolution of the current over the formation time. In momentum space this time evolution results in an integral equation for $\mathbf{F}(\mathbf{h}, p, \omega)$ which resums the influence of multiple soft scatterings⁸ on the emission process^{5,31}

$$\begin{aligned} 2\mathbf{h} &= i\delta E(\mathbf{h}, p, \omega)\mathbf{F}(\mathbf{h}) + \int \frac{d^2 k_{\perp}}{(2\pi)^2} \frac{\mathcal{C}_A(k_{\perp})}{2} \left\{ [\mathbf{F}(\mathbf{h}) - \mathbf{F}(\mathbf{h} - \omega\mathbf{k}_{\perp})] \right. \\ &\quad \left. + [\mathbf{F}(\mathbf{h}) - \mathbf{F}(\mathbf{h} + p\mathbf{k}_{\perp})] + [\mathbf{F}(\mathbf{h}) - \mathbf{F}(\mathbf{h} - (p - \omega)\mathbf{k}_{\perp})] \right\}. \end{aligned} \quad (41)$$

Finally, the full contribution to the Boltzmann equation takes the form of a gain term (reflecting the radiation from particles with momentum $p + \omega$) and a loss term (reflecting the radiation from the particle with longitudinal momentum p):^{29,34}

$$C_{\text{coll}} = \int_{-\infty}^{\infty} d\omega f_{p+\omega} \left. \frac{d\Gamma(p + \omega, \omega)}{d\omega} \right|_{\text{coll}} - \theta(p - 2\omega) f_p \left. \frac{d\Gamma(p, \omega)}{d\omega} \right|_{\text{coll}} \quad (42)$$

The region with $\omega < 0$ represents the collinear merging of two gluons to make a final state gluon. We also remark that Eq. (42) is finite in the infrared, as the power-law divergences for $\omega \rightarrow 0$ and $\omega \rightarrow p$ cancel between the gain and loss terms.

In practice, the integral equation for the bremsstrahlung rate (Eq. (41)) is most easily solved by working in coordinate space, which also illustrates the role of the coordinate space Wilson loop in shown in fig. 3. To facilitate this rewriting, we recall \mathbf{h}/p is conjugate to \mathbf{x}_{\perp} , which we relabel as \mathbf{b} . Dividing Eq. (41) by p and Fourier transforming with respect to \mathbf{h}/p we arrive at a coordinate space representation of the integral equation:

$$\begin{aligned} -2i\nabla\delta^2(\mathbf{b}) &= \frac{i}{2x(1-x)} (m_{\infty}^2(1-x+x^2) - \nabla_{\mathbf{b}}^2) \mathbf{f}(\mathbf{b}) \\ &+ \left(\frac{\mathcal{C}_A(x\mathbf{b})}{2} + \frac{\mathcal{C}_A(\mathbf{b})}{2} + \frac{\mathcal{C}_A((1-x)\mathbf{b})}{2} \right) \mathbf{f}(\mathbf{b}), \end{aligned} \quad (43)$$

where we have defined

$$\mathbf{f}(\mathbf{b}) = \int \frac{d^2 h}{(2\pi)^2 p^3} e^{i\frac{\mathbf{b}\cdot\mathbf{h}}{p}} \mathbf{F}(\mathbf{h}), \quad (44)$$

⁸Their effect on the emission process is usually called the Landau-Pomeranchuk-Migdal (LPM) effect.

and note that the integral entering the rate (40) becomes

$$\text{Re} \int \frac{d^2 h}{(2\pi)^2 p^4} 2\mathbf{h} \cdot \mathbf{F}(\mathbf{h}) = 2 \text{Im}(\nabla_b \cdot \mathbf{f}(0)). \quad (45)$$

This differential equation (Eq. (43)) can be solved to determine the bremsstrahlung rate.

The coordinate representation of the integral equation (Eq. (43)) naturally involves the Fourier-transformed collision kernel $\mathcal{C}_R(\mathbf{b})$ stemming from the Wilson line discussed above (see fig. 3 and Eq. (39)). Let us remark that the second line in Eq. (43) contains a sum of three two-body contributions, with the transverse distance b weighted by the ratio of two of the three energies p , ω and $p - \omega$. Indeed, it is easy to show^{31,35–38} that, at leading order, this is the only possibility. Beyond leading order, one could expect a more complicated three-pole structure, with three Wilson lines on the light cone, properly linked by transverse lines at their endpoints. However, at least up to NLO the symmetries of the system yield the simple planar dependence in the transverse plane reflected in Eq. (43).¹²

To summarize, we have identified three processes at leading order which are relevant to the transport of high momentum jet particles in a weakly coupled QGP. The first process is straightforward $2 \leftrightarrow 2$ collisions. This rate depends on the separation scale μ between the $\sim T$ scale, characterized by hard particles, and the $\sim gT$ scale, characterized by classical fields. The second process is momentum diffusion, which describes the interactions between the classical fields and the jet-particles. This process is described by a Fokker-Planck equation, whose parameters $\hat{e}(\mu)$ and $\hat{q}(\mu)$ also depend on the separation scale. However, the sum of the $2 \leftrightarrow 2$ collisions and the Fokker-Planck evolution is independent of μ . Finally, the third process is collinear bremsstrahlung, which is independent of the separation scale to this order. The parameters entering the collinear bremsstrahlung rate are the asymptotic masses m_∞^2 and the scattering kernel $\mathcal{C}(q_\perp)$. Both of these quantities can be expressed as (closely related) correlators of field strengths along the light cone, Eqs. (29), (39), and (80).

Anticipating Sec. 5, at next-to-leading order we will find corrections to the parameters of the Fokker-Planck equation, $\hat{e}(\mu)$ and $\hat{q}(\mu)$, and corrections to the parameters of the collinear bremsstrahlung rate, m_∞^2 and $\mathcal{C}(q_\perp)$. As we will see the NLO corrections to $\hat{e}(\mu)$ depend logarithmically on the separation scale μ . However, at NLO a correction to the collinear bremsstrahlung rate must also be included, which accounts for not-so-collinear emissions. This *semi-collinear* emission rate also depends on the separation scale μ , and the complete NLO rate is independent of μ . Thus, the NLO correction to the collision term takes the schematic form

$$\delta C = \delta C_{\text{coll}} + \delta C_{\text{diff}}[\mu] + \delta C_{\text{semi-coll}}[\mu]. \quad (46)$$

Before we describe these developments in detail, we will show how the computation of lightlike correlators in thermal field theory (such as $\hat{e}(\mu)$ and $\hat{q}(\mu)$) can be

dramatically simplified using the causal properties of these correlators. This is the task of the next section.

3. Hard Thermal Loops on the lightcone: a modern perspective

In the previous section we described a kinetic equation for jet-like particles based on $2 \leftrightarrow 2$ collisions, diffusion and drag, and collinear bremsstrahlung. The diffusion and drag coefficients are determined by classical statistical correlators of the soft background field on the light cone, Eq. (26) and Eq. (27). These correlation functions are to be evaluated using the Hard Thermal Loop (HTL) effective theory, which describes the response of the coupled Maxwell-Boltzmann system. Similarly, the collision kernel $C_R(\mathbf{q}_\perp)$ is also determined through Eq. (39) by the interaction between the classical particles and the the background field on the light cone.

Hard Thermal Loops involve a complex set of medium-modified propagators and vertices. Already at leading order the evaluation of the necessary correlators is seemingly complex. However, as we will describe in this section the evaluation of *lightcone* HTL correlators turns out to be surprisingly simple. For certain operators, such as those associated with transverse momentum diffusion Eq. (26), and soft corrections to the asymptotic mass, a Euclidean formalism can be used.¹² On the other hand, other operators such as those associated with longitudinal diffusion and drag are surprisingly insensitive to the $\sim gT$ sector, and lead to contact terms which correct the collinear emission.

These simplifications are a consequence of the following physical picture. Since the hard and jet-particles are propagating almost exactly along the light cone, they are probing an essentially undisturbed plasma, at least as far as the soft classical background is concerned. Thus, the soft correlations that are probed by are the hard and jet-particles are statistical rather than dynamical, *i.e.* these are correlations that arise from the partition function, rather than a retarded response averaged over the correlated initial conditions determined by the partition function. This heuristic explanation underlies the dimensionally-reduced lattice calculation of \hat{q} which is described in Sec. 4.

At a technical level, these simplifications were first realized using light cone causality of retarded propagators,¹² which says that

$$G_R(p^+, p^-, \mathbf{p}_\perp) = \int dx^+ dx^- d^2x_\perp e^{i(p^+x^- + p^-x^+ - \mathbf{p}_\perp \cdot \mathbf{x}_\perp)} G_R(x^+, x^-, \mathbf{x}_\perp) \quad (47)$$

is an analytic function of p^+ in the upper half-plane at fixed p^- and p_\perp . This is because the retarded response function is only non-zero in the forward light cone $2x^+x^- \geq x_\perp^2$. Thus the integral in Eq. (47) has support only for $x^- > 0$, and the Fourier integral provides an analytic continuation in the upper half p^+ plane, due to the decreasing exponential $e^{ip^+x^-}$. To illustrate these simplifications in a concrete context, we will evaluate the drag and transverse momentum diffusion coefficients, Eq. (26) and Eq. (27), at leading order. To do this we will first briefly review Hard

Thermal Loops in Sec. 3.1. Then we will use the HTL theory to evaluate Eq. (26) and Eq. (27) in Sec. 3.2 and Sec. 3.3, using light cone causality to simplify the calculation.

3.1. Hard Thermal Loops and Light Cone Correlation Functions

To briefly describe the Hard Thermal Loops consider a scalar field ϕ_a transforming in the representation R (where a is a color index). There is a single particle density matrix $N_{ba}(t, \mathbf{p}, \mathbf{x})$ transforming in the $R \times \bar{R}$ representation which records the statistics of the color orientations of a quasi-particle excitation. Heuristically,³⁹ $N_{ba}(t, \mathbf{p}, \mathbf{x})$ is a quasi-local expectation value of $\langle a_{a,\mathbf{p}}^\dagger(t, \mathbf{x}) a_{b,\mathbf{p}}(t, \mathbf{x}) \rangle$ at the space time point (t, \mathbf{x}) . More formally, $N_{ba}(t, \mathbf{p}, \mathbf{x})$ can be defined as the Wigner transform of the gauge-covariant Wightman function.¹⁰ The gluon singlet distribution function (denoted $n_{\mathbf{p}}$ above) is proportional to the color trace of a single particle density matrix,

$$n_{\mathbf{p}} \equiv \frac{1}{d_R} \text{Tr} [N(t, \mathbf{x}, \mathbf{p})] \quad (48)$$

while the color current associated with the gluon distribution is^h

$$J^{A,\mu}(t, \mathbf{x}) = 2g \int \frac{d^3\mathbf{p}}{(2\pi)^3} \text{Tr} [T^A N(t, \mathbf{x}, \mathbf{p})] v_{\mathbf{p}}^\mu, \quad (49)$$

where $v_{\mathbf{p}}^\mu = (1, \hat{\mathbf{p}})$. The single particle density matrices N_{ba} obey a Vlasov equation

$$(D_t + \mathbf{v} \cdot \mathbf{D}_{\mathbf{x}}) N_{\mathbf{p}} + \frac{1}{2} g \left\{ (\mathbf{E} + \mathbf{v} \times \mathbf{B})_i, \frac{\partial N_{\mathbf{p}}}{\partial p_i} \right\} = 0, \quad (50)$$

where $D_\mu = \partial_\mu - ig[A_\mu, \cdot]$ denotes the appropriated gauge covariant derivative for the $R \times \bar{R}$ representation, and the curly brackets denote an anti-commutator. The particles source the classical chromo-electric and magnetic fields

$$-D_\mu F^{\mu\nu}(t, \mathbf{x}) = J^\nu(t, \mathbf{x}). \quad (51)$$

The Hard Thermal Loop retarded Green function is derived from this Maxwell-Boltzmann system of equations, Eq. (50) and Eq. (51), by expanding around the equilibrium state, $n_{\mathbf{p}} = 1/(e^{E_{\mathbf{p}}/T} - 1)$

$$N_{ba} = n_{\mathbf{p}} \delta_{ba} + \delta N_{ba}, \quad (52)$$

$$A_\mu = 0 + \delta A_\mu, \quad (53)$$

and solving for the response of the classical field to an external current, $A^\mu(\omega, \mathbf{q}) = iG_R^{\mu\nu}(\omega, \mathbf{q}) J_{\nu, \text{ext}}(\omega, \mathbf{q})$. We will not go through this set of steps but refer to the

^hThe leading factor of 2 is the spin of the gluon, and for a scalar field this factor would not appear.

literature.^{10,40} The resulting retarded Green functions in the Coulomb gauge are

$$G_R^{00}(\omega, \mathbf{q}) = \frac{-i\eta^{00}}{q^2 + \Pi_L(q^0/q)} \Big|_{q^0=\omega+i\epsilon}, \quad (54a)$$

$$G_R^{ij}(\omega, \mathbf{q}) = \frac{-i(\delta^{ij} - \hat{q}^i \hat{q}^j)}{-(q^0)^2 + q^2 + \Pi_T(q^0/q)} \Big|_{q^0=\omega+i\epsilon}, \quad (54b)$$

where $\eta^{00} = -1$ and the self-energies are

$$\Pi_L(x) = m_D^2 \left(1 - \frac{x}{2} \log \left(\frac{x+1}{x-1} \right) \right), \quad (55a)$$

$$\Pi_T(x) = \frac{m_D^2}{2} \left(x^2 - \frac{(x^2-1)x}{2} \log \left(\frac{x+1}{x-1} \right) \right), \quad (55b)$$

with $x = q^0/q$. The spectral density is the difference between the retarded and advanced green functions

$$\rho^{\mu\nu}(\omega) = G_R^{\mu\nu}(\omega, \mathbf{q}) - G_A^{\mu\nu}(\omega, \mathbf{q}), \quad (56)$$

where $G_A(\omega, \mathbf{q})$ is found by setting $q^0 = \omega - i\epsilon$ in Eq. (54). The HTL spectral density and its properties are discussed in the references.¹⁰

As we described above, \hat{q} and \hat{q}_L are determined by the propagation of the hard and jet particles in a random classical background field. In equilibrium, the fluctuation-dissipation theorem relates the symmetrized two point function $G_{rr}(\omega, \mathbf{q})$ to the imaginary part of the retarded responseⁱ

$$G_{rr}^{\mu\nu}(\omega, \mathbf{q}) \equiv \frac{1}{2} \langle \{A^\mu(\omega, \mathbf{q}), A^\nu\} \rangle = \left(n_B(\omega) + \frac{1}{2} \right) \rho^{\mu\nu}(\omega, \mathbf{q}). \quad (57)$$

For a classical background field A_μ , the symmetrization of the field operators is irrelevant, and the symmetrized two point function simply records the two-point statistics of the classical field. Approximating Eq. (57) for $\omega \ll T$ yields

$$G_{rr}^{\mu\nu}(\omega, \mathbf{q}) = \langle A^\mu(\omega, \mathbf{q}) A^\nu \rangle = \frac{T}{\omega} \rho_{HTL}^{\mu\nu}(\omega, \mathbf{q}). \quad (58)$$

We will use these statistics of the classical soft modes when evaluating the longitudinal drag and diffusion coefficient in the next section.

In addition to these rather complex propagators, the Maxwell-Boltzmann system leads to additional HTL vertices which describe how the soft classical background interacts with itself. The resulting Feynman rules describing this response are rather complex as well. To date, this elaborate set of Feynman vertices has been used to compute the dilepton emission rate at small invariant mass⁴² and the diffusion coefficient of a heavy quark at NLO.⁴³ As discussed above and in the next sections, these intricate HTL rules simplify dramatically when evaluating the lightcone correlators involved in energy loss. Indeed, the NLO computations of energy loss described in Sec. 5 would not have been possible without these simplifications.

ⁱOur notation G_{rr} follows the one of the so-called r/a formalism of Thermal Field Theory. We refer to this reference⁴¹ for a comprehensive set of Feynman rules for the HTL theory in that formalism.

3.2. Transverse diffusion and Euclidean operators

In this section we will compute \hat{q} and $\mathcal{C}(q_\perp)$ at LO using Eqs. (26), (35) and (39) as our starting point. Recall that these Wilson line correlators describe the propagation of a hard or jet particle traversing the classical field provided by the soft modes. The statistics of these classical fluctuations are given by Eqs. (57) and (58). As we will see, light cone causality Eq. (47) dramatically simplifies the calculation, leading to a Euclidean formulation.

For \mathcal{C} , applying the definition (39), one finds (in any non-singular gauge) that the diagrams in Fig. 4 contribute. Clearly, the diagram on the right and its symmetric

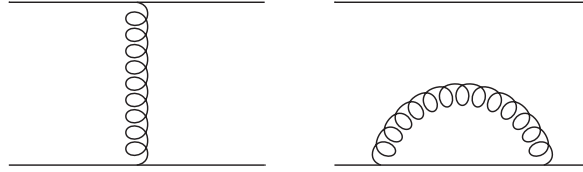


Fig. 4. Diagrams for the leading-order evaluation of $\mathcal{C}(x_\perp)$ in a non-singular gauge. The plain lines represent the Wilson lines along the light-cone, at transverse separation x_\perp . The diagram with the self-energy on the upper Wilson line is not shown.

give rise to the x_\perp -independent part in Eq. (38), whereas the one on the left gives rise to the x_\perp -dependent exponential, so that, at leading order, for an adjoint source (a gluon) one has

$$\mathcal{C}(q_\perp) = g^2 C_A \int \frac{dq^0 dq_z}{(2\pi)^2} 2\pi \delta(q^0 - q_z) G_{rr}^{--}(Q), \quad (59)$$

$$\mathcal{C}(x_\perp) = \int \frac{d^2 q_\perp}{(2\pi)^2} (1 - e^{i\mathbf{x}_\perp \cdot \mathbf{q}_\perp}) \mathcal{C}(q_\perp), \quad (60)$$

where $G_{rr}^{--}(Q) = v_\mu v_\nu G_{rr}^{\mu\nu}(Q)$ is given for soft momenta by Eq. (58). Since $q^0 = q^z$ enforces space-like kinematics, it would then seem that one is left with an integral of the non-trivial HTL spectral function Eq. (56) over the entire Landau cut, $|q^0| < q$. Such integral poses no particular challenge numerically,⁴⁴ but any extension beyond leading order, with loops composed of HTL propagators and vertices generated by the rules discussed in the previous section 3.1, would be extremely challenging from the computational viewpoint. We refer to the computation to NLO⁴³ of κ , the analogue of \hat{q} for a very massive quark, for an example of such an intricate calculation. In the present case, however, there is a considerable simplification. As we have remarked in Sec. 2, $\mathcal{C}(q_\perp)$ can be obtained from a Wilson loop supported on a light front (a null plane), as show in Fig. 3. The special analyticity properties of objects of this kind are the key to their simplification. Indeed, Alves, Das and Perez,⁴⁵ and Weldon,^{46,47} introduced the technique of light-front quantization into Euclidean Thermal Field Theory, extending the usual imaginary time formalism

from the space-like domain to light fronts. Subsequently, and independently, Caron-Huot¹² introduced a similar quantization technique and showed how it can reduce the calculation of (the soft contribution to) this Wilson loop to a much simpler Euclidean calculation in dimensionally-reduced EQCD.

The first step in this endeavor consists in showing that the calculation of n -point correlation functions, where all fields lie on a spacelike hypersurface, can be carried out by Euclidean techniques.^{12,45,46} The null correlators we need can also be computed provided that they are free of collinear singularities, which they are up to NLO included.¹² The proofs presented in Refs.^{12,45,46} are rather complex and technical. Here we will present a much simpler derivation, also due to Caron-Huot^j, already collected in¹⁴, which we follow closely. It is an illustration of the two-point function case, which, as one can see from Eq. (59), will nicely yield the LO result for $\mathcal{C}(q_\perp)$.

Consider the symmetrized correlator of some operator (such as G^{--} in our case), $G_{rr}(x^0, \mathbf{x})$ with $|x^z| > |x^0|$. Since the separation is spacelike, operators commute, and therefore G_{rr} equals $G^<$, or $G^>$, as shown in Eq. (58). We are interested in the lightlike limit $x^z = x^0$. There are additional subtleties in taking this limit, but these are irrelevant for the soft and leading order contributions to such correlators. Let us write G_{rr} in terms of its Fourier representation, i.e. the inverse of Eq. (47)

$$G_{rr}(x^0, \mathbf{x}) = (2\pi)^{-4} \int d\omega \int dp^z d^2 p_\perp e^{i(x^z p^z + \mathbf{x}_\perp \cdot \mathbf{p}_\perp - \omega x^0)} G_{rr}(\omega, p^z, p_\perp), \quad (61)$$

and use the exact relation between the spectral function and the symmetric propagator, Eq. (57). We then shift one integration variable to $\tilde{p}^z = p^z - (x^0/x^z)\omega$:

$$G_{rr}(x^0, \mathbf{x}) = \int \frac{d\omega d\tilde{p}^z d^2 p_\perp}{(2\pi)^4} e^{i(x^z \tilde{p}^z + \mathbf{x}_\perp \cdot \mathbf{p}_\perp)} \left(n_B(\omega) + \frac{1}{2} \right) \rho(\omega, \tilde{p}^z + \omega(x^0/x^z), p_\perp), \quad (62)$$

so that the Fourier exponent is now frequency-independent and we can perform the ω integration by contour methods. The spectral weight is written as

$$\rho(\omega, \mathbf{p}) = G_R(\omega, \mathbf{p}) - G_A(\omega, \mathbf{p}), \quad (63)$$

and the integral over $G_R(\omega, p)$ is performed by closing the contour in the upper half plane, while the integration of $G_A(\omega, p)$ is performed by closing the contour in the lower half plane. Since $|x^0/x^z| < 1$, $G_R(\omega, \tilde{p}^z + \omega(x^0/x^z), p_\perp)$ is an analytic function of ω in the upper complex ω plane. This is a consequence of (slightly generalized) light-cone causality^k as described in and after Eq. (47). The advanced function is similarly an analytic function in the lower complex ω plane. Therefore the only singularities encountered in continuing the frequency integration are those in the statistical function $(n_B(\omega) + 1/2)$, which has poles at $\omega_n = 2\pi i n T$ with

^jS. Caron-Huot, oral presentation at the Institute for Nuclear Theory (Seattle), 29 March 2012

^kThis is precisely a statement of lightcone causality as described in Eq. (47) when $x^0/x^z = 1$. In this case, $\tilde{p}^z = -p^-$ and ω parametrizes the analytic continuation in p^+ at fixed p^- and p_\perp .

$n = (\dots - 1, 0, 1, \dots)$ and residues equal to T . Closing the contour around these poles, and renaming \tilde{p}^z to p^z , we find¹

$$G_{rr}(x^0, \mathbf{x}) = T \sum_n \int \frac{d^3p}{(2\pi)^3} e^{i\mathbf{x}\cdot\mathbf{p}} G_E \left(\omega_n, p^z + i\omega_n \frac{x^0}{x^z}, p_\perp \right), \quad \omega_n = 2\pi nT, \quad (64)$$

where we have recalled that the retarded green function is determined by an analytic continuation of the Euclidean function, $G_R(\omega, p) = -iG_E(\omega_E = -i(\omega + i\epsilon), p)$.

When we need to compute the soft gT contribution to such a correlator, one may drop the nonzero Matsubara frequency contributions; that is, we keep only the $n = 0$ term in the sum. This term, $G_E(\omega_n, p^z + i\omega_n(x^0/x^z), p_\perp) \rightarrow G_E(0, p^z, p_\perp)$, is the Euclidean correlation function of the 3-dimensional dimensionally reduced EQCD theory, which we shall describe in more detail in Sec. 4. Thus, the soft contribution to Euclidean operators at spacelike and lightlike separations is time-independent.

Let us go back to the computation of $\mathcal{C}(x_\perp)$. As all points in that Wilson loop are either at a space-like or light-like separation, the above introduced EQCD reduction is applicable. Hence, at leading order, Eq. (59) becomes

$$\mathcal{C}(q_\perp) = g^2 C_A T \int \frac{dq_z}{(2\pi)} 2\pi \delta(q_z) G_E^{--}(0, q_z, q_\perp) = g^2 C_A T \left(\frac{1}{q_\perp^2} - \frac{1}{q_\perp^2 + m_D^2} \right), \quad (65)$$

The result is easily understood as the difference between the massless, transverse and massive, longitudinal EQCD propagators, which also arise as the $q^0 = q^z = 0$ limit of Eq. (54). For (the soft contribution to) \hat{q} we then have the well-known logarithmic dependence on the cut-off, which we anticipated in Eq. (22) in Sec. 2, i.e.

$$\hat{q}(\mu) = g^2 C_A T \int^\mu \frac{d^2 q_\perp}{(2\pi)^2} \frac{m_D^2}{q_\perp^2 (q_\perp^2 + m_D^2)} = \frac{g^2 C_A T m_D^2}{2\pi} \ln \frac{\mu}{m_D}. \quad (66)$$

Furthermore, we remark that Eq. (65) was already obtained⁴⁸ using a sum rule. Caron-Huot has shown¹² that the two approaches are equivalent, and that the sum rule is possible because of the aforementioned analyticity of retarded and advanced functions. These very same properties will be of great importance for the evaluation of non-Euclidean operators.

Finally, let us consider the effect of the non-zero Matsubara modes we have neglected in Eq. (65). If $q_\perp \sim gT$ is kept soft, the subtleties in putting $x^0/x^z = 1$ will need to be reexamined when including the non-zero Matsubara modes in the sum. The evaluation of these contributions is related to the collinear singularities that should show up at NNLO. It would be interesting to clarify these collinear singularities with direct calculations. If one considers shorter transverse separations (with $q_\perp \sim T$) then all Matsubara modes will contribute straightforwardly, and the Euclidean light-front computation in Eq. (64) may be more cumbersome than a direct computation in the real-time formalism. The leading-order contribution to \hat{q} from the scale T has been computed²⁶ using real time methods.

¹ The pole at $n = 0$ is an artifact of the separation of ρ , which vanishes for $\omega = 0$, into G_R and G_A . The individual poles there can then be dealt with in a principal value prescription, for instance.

3.3. Longitudinal diffusion and non-Euclidean operators

As we mentioned at the beginning of Sec. 3, not all lightcone or light-front supported operators admit a three-dimensional, Euclidean description for the soft modes. A prime example is the longitudinal momentum diffusion coefficient \hat{q}_L , as given by Eq. (27). At leading order it is given by the diagram shown in Fig. 5. In any

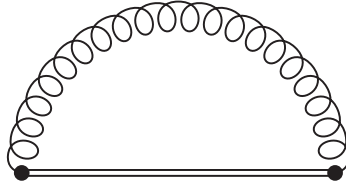


Fig. 5. The leading-order soft contribution to \hat{q}_L . The two dots are the two field strengths and the double line is the adjoint Wilson line connecting them. The curly line is a soft HTL gluon.

non-singular gauge it reads

$$\hat{q}_L = g^2 C_A \int_{-\infty}^{+\infty} dx^+ \int \frac{d^4 Q}{(2\pi)^4} e^{-iq^- x^+} (q^+)^2 G_{rr}^{--}(Q), \quad (67)$$

where again $G_{rr}^{--}(Q)$ is given by Eq. (58). The x^+ integration sets q^- to zero. We clearly see that, although originating from a lightcone operator, q^+ cannot be evaluated in EQCD: indeed, the zero-mode contribution exactly vanishes when the previous techniques are applied.

We can however evaluate Eq. (67) by employing sum rules that are rooted in the same analyticity properties that were used in the derivation of Eq. (64). In detail, we plug the result of Eq. (58) in Eq. (67). Up to $\mathcal{O}(g^2)$ corrections^m we then have

$$\hat{q}_L = g^2 C_A \int \frac{dq^+ d^2 q_\perp}{(2\pi)^3} T q^+ (G_R^{--}(q^+, q_\perp) - G_A^{--}(q^+, q_\perp)). \quad (68)$$

This too would be a simple enough numerical integral⁴⁹ over the HTL spectral function in the Landau cut, of difficult extension to higher orders. However, as we have previously remarked, retarded (advanced) two-point functions are analytic in the upper (lower) half-plane in any timelike or light-like variable. We can thus deform the integration contours¹⁶ away from the real axis onto \mathcal{C}_R ($|q^+| = \mu^+ \gg gT$, $\text{Im } q^+ > 0$) and \mathcal{C}_A ($|q^+| = \mu^+ \gg gT$, $\text{Im } q^+ < 0$), as depicted in Fig. 6.ⁿ μ^+ is a

^mWhen expanding the statistical factor in the soft region in Eq. (58), one has $n_B(\omega) + 1/2 = T/\omega(1 + \mathcal{O}(g^2))$.

ⁿThe longitudinal and transverse contributions to $G_R^{--}(Q)$ contain poles at $q^+ = q^-/2 \pm iq_\perp$ ($q^2 = 0$), which, being on both sides of the complex plane, appear to violate analyticity. However their residue cancels in the sum of longitudinal and transverse components. As observed in¹², they are artifacts of the decomposition into Lorentz-variant longitudinal and transverse modes and their contribution has to vanish in all gauge-invariant quantities.

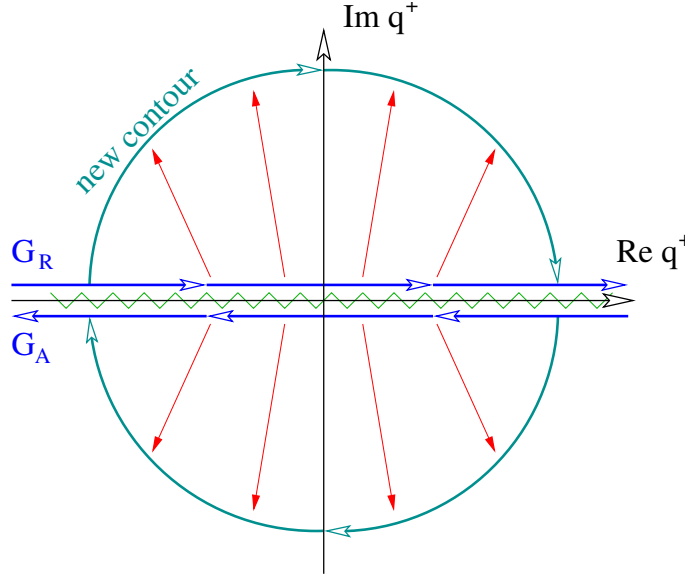


Fig. 6. Integration contour in the complex q^+ integration, and the deformation we use to render $q^+ \gg gT$. G_R runs above the real axis and G_A below.

UV cutoff on q^+ , to make sure that we consider only the soft region. As we shall see, it will have no effect.

Along the arcs q^+ is then large, albeit complex. The longitudinal and transverse propagators simplify greatly, i.e.

$$G_R^{--}(q^+, q_\perp) = G_R^L(q^+, q_\perp) + \frac{q_\perp^2}{q^2} G_R^T(q^+, q_\perp) \quad (69)$$

$$= \frac{i}{(q^+)^2} + \frac{q_\perp^2}{(q^+)^2} \frac{-i}{q_\perp^2 + m_\infty^2} + \mathcal{O}\left(\frac{1}{(q^+)^3}\right), \quad (70)$$

where we have used the Coulomb gauge propagators given in Eq. (54) and $m_\infty^2 = m_D^2/2$ is the LO gluon asymptotic thermal mass as given in Eq. (8). What this equation is telling us is that, for large (complex) q^+ , the longitudinal part is unchanged with respect to its unresummed version, whereas the transverse part acquires the asymptotic mass, which is typical of collinear, transverse excitations.

Upon plugging Eq. (70) in Eq. (68), the q^+ integration along the arcs is trivial and the end result is¹⁶

$$\hat{q}_L(\mu) = g^2 C_A T \int^\mu \frac{d^2 q_\perp}{(2\pi)^2} \frac{m_\infty^2}{q_\perp^2 + m_\infty^2} = \frac{g^2 C_A T}{2\pi} m_\infty^2 \ln \frac{\mu}{m_\infty}, \quad (71)$$

where contributions smaller than $1/(q^+)^2$ in Eq. (70) are not needed, as they would only give rise to power-law terms in the cutoff on q^+ , which would then cancel against contributions from larger scales. The transverse integration has been regulated in the UV with $\mu \gg gT$, as in Eq. (66). Again, this result had been anticipated

in Eq. (22). As we commented after Eq. (16), this calculation, together with the one in the previous subsection, clearly shows the physical reasons causing the Debye mass m_D to appear in $\hat{q}(\mu)$ and the asymptotic mass m_∞ to appear in $\hat{q}_L(\mu)$.

The sum rule we have just illustrated has been derived in this fashion in¹⁶. It can also be seen as the bosonic equivalent of the one presented in the calculation of the thermal photon rate to NLO¹⁴ and of the thermal ultrarelativistic right-handed neutrino rate at LO.⁵⁰ We also remark that the same result (71) was previously obtained in a different way⁵¹ for the drag coefficient \hat{e} , which is related by the Einstein relation Eq. (17). As it is shown there,⁵¹ once the difference in regularization between $q_\perp < \mu_\perp$ and $q < \mu_q$ is taken into account, Eq. (71) agrees with the numerical results of Braaten and Thoma⁴⁹ for $v \rightarrow 1$.

In summary, in this Section we have introduced Hard Thermal Loops and their simplification on the light cone. In Sec. 3.2 we have analyzed the subset of operators, including transverse momentum diffusion, that admit a three-dimensional, Euclidean description in the soft region, whereas in the current subsection we have analyzed those that do not, showing how they still considerably simplify. In the following Section we will show how Euclidean operators can be calculated on the lattice, whereas in Sec. 5 we will use the results of this Section to generalize the perturbative kinetic approach to NLO.

4. Non-perturbative determinations of $\mathcal{C}(x_\perp)$ and \hat{q}

As we mentioned previously, the field-theoretical developments introduced by Caron-Huot¹² make it possible to map certain operators supported on light fronts and light cones to the Euclidean domain, where the soft contribution is dominated by the dimensionally reduced zero modes of 3D EQCD. Recently, this has been exploited to compute the soft contribution to $\mathcal{C}(x_\perp)$ and \hat{q} on the lattice. Laine and Rothkopf⁵² have performed a first study of the Wilson loop defined in Fig. 3 in classical gauge theory, which allows real-time lattice studies and catches the qualitative nature of the soft physics, which, as we have argued in Sec. 2, is of classical origin. In particular, they also examined the dependence on v of the Wilson loop (i.e. whether the approach to the light-cone from above or below is different for classical fields), finding it modest.

Panero, Rummukainen and Schäfer¹³ have instead computed the soft contribution to $\mathcal{C}(x_\perp)$ and to \hat{q} by means of lattice simulations of EQCD.^o In the remainder of this Section, we will illustrate the basic principles of this treatment and its potential application to other light-cone observables that are suited to it, such as $\hat{q}(\delta E)$, which will be defined in Sec. 5, or the asymptotic masses. To this end, we start by reviewing Electrostatic QCD (EQCD),^{54–58} which is a dimensionally-reduced EFT of QCD describing the time-independent, long-wavelength $\lambda \sim 1/(gT)$ modes of the

^o A different method, not based on the properties of Sec. 3, for estimating \hat{q} on the lattice has been proposed.⁵³

latter theory. If treated perturbatively, it breaks down at very long wavelengths (very small momenta) $\lambda \sim 1/(g^2 T)$ ($k \sim g^2 T$) where magnetic non-perturbative contributions^{54,59} appear. If, on the other hand, it is treated non-perturbatively, both the electric and magnetic scales are treated correctly. Hence, a lattice calculation in EQCD, such as the one of \hat{q} we are considering, determines the soft (gT) and ultrasoft ($g^2 T$) contributions. Indeed, nonperturbative EQCD has been employed for many studies of the thermodynamics of QCD, as in this example,⁶⁰ and of the gauge sector of the standard model, as in this review⁶¹ and this recent work.⁶²

The Lagrangian of EQCD reads

$$\mathcal{L} = \frac{1}{4} F_{ij}^a F_{ij}^a + \text{Tr}((D_i A_0)^2) + m_E^2 \text{Tr}(A_0^2) + \lambda_3 (\text{Tr}(A_0^2))^2, \quad (72)$$

where only operators of dimension up to three have been kept. $D_i = \partial_i - ig_E[A_i, \cdot]$ is the standard covariant derivative, so that the Lagrangian describes a 3D SU(3) Yang-Mills field minimally coupled to an adjoint scalar field A_0 , which has a mass and a quartic coupling (adjoint Higgs). Fermions, having only odd Matsubara frequencies proportional to πT , are completely integrated out in the dimensional reduction.

At leading order the matching between QCD and EQCD yields^{54,56,58}

$$g_E^2 = g^2(\mu)T, \quad m_E^2 = \left(\frac{N_c}{3} + \frac{n_f}{6}\right) g^2(\mu)T^2, \quad \lambda_3 = \frac{9 - n_f}{24\pi^2} g^4(\mu)T, \quad (73)$$

where g_E is the dimensionful coupling of EQCD and $g(\mu)$ is the scale-dependent coupling of QCD. The mass parameter is equal to the leading-order Debye mass. The positive dimensionality of g_E makes the theory super-renormalizable.

The EQCD action can be readily discretized for lattice studies. We refer to^{13,60} for details on this procedure. The implementation of the Wilson loop^{12,32,33} depicted in Fig. 3 is on the other hand somewhat non-trivial in the dimensionally-reduced theory, where the time dimension is integrated out. In the continuum, the Wilson line along the light-cone direction changes from

$$U(x_f^+; x_i^+) = \mathcal{P} \exp \left[-ig \int_{x_i^+}^{x_f^+} dx^+ (A^0(x^+) - A^z(x^+)) \right] \text{ in Minkowskian QCD}, \quad (74)$$

to

$$U(x_{z,f}; x_{z,i}) = \mathcal{P} \exp \left[-ig \int_{x_{z,i}}^{x_{z,f}} dx_z (iA_0(x_z) - A_z(x_z)) \right] \text{ in EQCD}, \quad (75)$$

where the A^0 in Eq. (74) is the temporal gauge field of Minkowskian 4D QCD, whereas the one in Eq. (75) is the adjoint scalar of Euclidean, 3D EQCD, the extra i coming from the Wick rotation. The other coordinates (\mathbf{x}_\perp and, in Eq. (74), x^-) are understood to be constant and are not shown.

The lattice version of Eq. (75) is also non-trivial, because in the discretized action the 3D gauge fields are naturally re-expressed as gauge links between the

lattice sites, while the A_0 scalar field is defined on the lattice sites. This leads to, in the notation of¹³

$$L_3(x, an_\ell) = \prod_{n=0}^{n_\ell-1} U_3(x + an\hat{3}) H(x + a(n+1)\hat{3}), \quad (76)$$

where L_3 is the lattice equivalent of Eq. (75), with $n_\ell = \ell/a$ the length of the Wilson line in units of the lattice spacing a . U_3 is a gauge link in the z direction and $H(x)$ is a Hermitian, rather than unitary, matrix obtained by exponentiation of $A_0(x)$, i.e.

$$H(x) = \exp[-ag_E^2 A_0(x)]. \quad (77)$$

Note that $H(x)$ represents a parallel transporter along a *real-time* interval of length a . The transverse Wilson lines L_1 are instead the usual product of gauge links, so that, schematically, the Wilson loop takes the form depicted in Fig. 7.

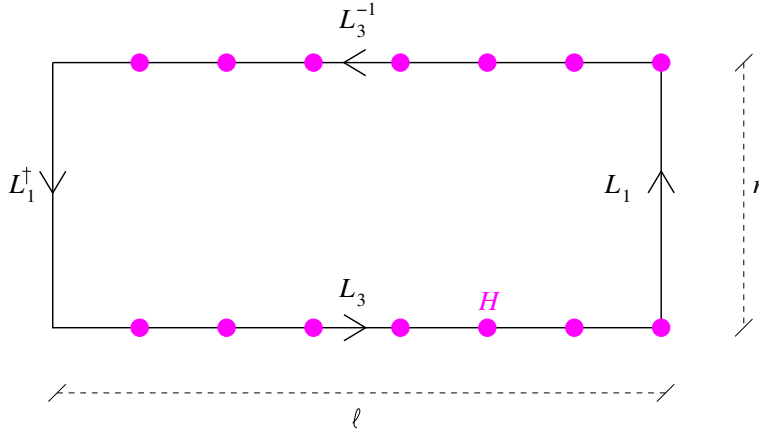


Fig. 7. The Wilson loop yielding $\mathcal{C}(x_\perp = r)$ in EQCD. The dots on the lines in the horizontal direction represent the insertion of the Hermitian operator H at the lattice sites, whereas the lines connecting them are the gauge links in the z direction. Figure taken from the original reference.¹³

The lattice measurements¹³ of $\mathcal{C}(x_\perp)$ through the above definition are summarized in Fig. 8. As the authors remarked, once the value the Debye mass which includes the non-perturbative relative $\mathcal{O}(g)$ correction⁶³ is used to set the scale and as input for the perturbative calculation of Caron-Huot, the agreement between lattice and perturbation theory becomes surprisingly good. If, on the other hand, the perturbative Debye mass is used, perturbation theory yields a significantly smaller $\mathcal{C}(x_\perp)$ at intermediate distances.

The soft contribution to \hat{q} can then be extracted from the short-distance behavior of $\mathcal{C}(x_\perp)$ along the line of Eq. (37), i.e. ^{12,14,64}

$$\mathcal{C}(x_\perp) \xrightarrow{x_\perp m_D \ll 1} c_1 x_\perp + \hat{q}_{\text{soft}} \frac{x_\perp^2}{4} + \mathcal{O}(x_\perp^3). \quad (78)$$

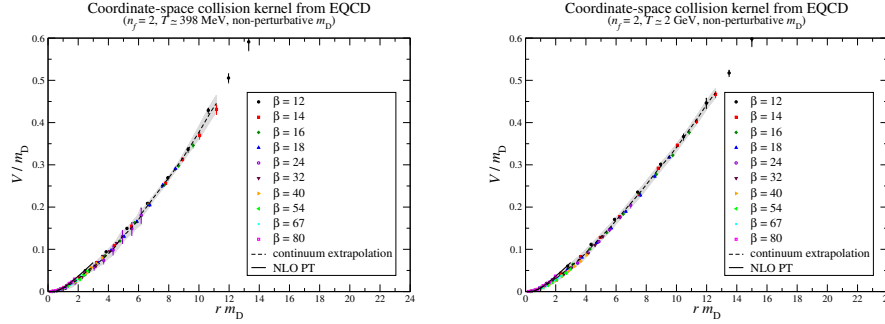


Fig. 8. Results for $\mathcal{C}(x_\perp)$ at two different values of the temperature. The Debye mass used as a scale for the axes and plugged in the NLO perturbative calculation¹² is the non-perturbative one.⁶³ Figure taken from the original reference.¹³

The \hat{q}_{soft} extracted in this way also contains a residual logarithmical dependence on x_\perp , reflecting the leading-order UV divergence of \hat{q}_{soft} (see Eq. (66)) that is absorbed by the hard contribution. We refer to^{13,64} for further details on the matching procedure and the addition of the leading-order hard contribution.²⁶ Once this has been performed, Panero *et al.* report an estimate for \hat{q} of 6 GeV²/fm at their lower temperature of 398 MeV, with an estimated uncertainty of 15 to 20%. We remark that higher-order contributions from the hard scale, as well as the possible collinear contribution mentioned in Sec. 3.3, are absent from this determination.

A possible limitation to the approach we have outlined is that it relies on a separation of scale between the hard particles, with momenta of order πT , and the soft and ultrasoft fields, characterized by gT and g^2T . However, as the authors remark, the literature suggests (see for instance^{60,65,66}) that analytical computations relying on this separation of scales may be sufficiently accurate down to low temperatures, perhaps, suprisingly, down to⁶⁷ $T \sim 2T_c$.

It is worth remarking that the NLO perturbative calculation predicts at the origin a negative linear slope,^P i.e. $c_i < 0$ in Eq. (78), which is not observed in the lattice calculation. This can be attributed to discretization errors, which are more severe at short distances, corresponding to the UV region $p_\perp \gg m_D$ in momentum space. At leading order in PT, the dominant UV behavior ($1/p_\perp^2$) cancels between the longitudinal and transverse one-gluon exchanges, as shown in Eq. (65), leaving a m_D^2/p_\perp^4 correction. This cancellation, while exact in the continuum, is only approximate on the lattice. D'Onofrio, Kurkela and Moore⁶⁸ have estimated the associated error to be of order a/x_\perp and hence especially relevant at short distances. Their computation of the renormalization properties of Eq. (76) to order a can help alleviating these discretization effects.

^PDue to the super-renormalizability of EQCD, each loop order causes a different power-law behavior for \mathcal{C} , so that higher orders cannot contaminate this effect.

We also note that, by comparing their results with the estimate of the magnetic contribution only to \hat{q} ,^{33,64} which can be performed similarly by simulating a Wilson loop in the pure 3D gauge theory, Panero *et al.* have been able to establish that the magnetic contribution (g^2T only) is subleading compared to the full non-perturbative EQCD determination, which includes the gT and g^2T contributions.

Future directions for this very promising new direction can include more refined measurements of \hat{q} , for instance improving the approach to the continuum at short distances along the lines discussed before or extending the range of explored temperatures. An altogether similar approach can be used to determine non-perturbatively the soft contribution to other operators that are amenable to a Euclidean treatment, such as $\hat{q}(\delta E)$ or the condensates appearing in the definition of the asymptotic masses (see Sec. 5.1). One could then envisage for the future the establishment of a factorization program for the computation of jet-related observables: the soft physics, where pQCD struggles, is encoded into these effective operators measured on the lattice, whereas the harder scales are treated perturbatively.⁹ EFT techniques could be used to make the factorization well defined and deal with possible large logarithms. A first step in this direction has been taken in this study.⁷⁰ It compares the screening masses of a specific correlator, extracted from lattice measurements, with their determination through a differential equation that is very similar to Eq. (43), up to a complex phase for $\mathcal{C}(x_\perp)$. By using the lattice determination of the latter the authors find a very good agreement with the non-perturbative screening masses.

5. Perturbative next-to-leading order

As we have anticipated, the recent technological developments outlined in Sec. 3 make the extension to next-to-leading order of the kinetic approach sketched in Sec. 2 possible. In that Section we have introduced the three fundamental processes that make up the leading-order collision operator, i.e. diffusion, large-angle scatterings and collinear splittings/joinings. Next-to-leading order contributions represent a relative $\mathcal{O}(g)$ correction and come about because, as we have mentioned, soft gluons are highly occupied, with $n_B(q^0 \sim gT) \approx T/q^0 \sim 1/g$. For this reason one can show that loops composed of soft propagators only are suppressed by a factor of g rather than g^2 , giving rise to *soft loop corrections*. Another source of $\mathcal{O}(g)$ corrections comes from regions of the LO calculation where a gluon becomes soft, without being properly treated, i.e. with HTL resummations. For instance, in large-angle scatterings, the integrations over the energies of the incoming and outgoing gluons stretch down to zero, including an $\mathcal{O}(g)$ region of phase space where they are soft, but treated as massless, rather than HTL, excitations. At NLO one then needs to replace the improper LO evaluation of these *mistreated regions* with the proper one.

⁹ A factorized approach sharing the same spirit, but using holographic methods for the description of the medium, has recently been presented in⁶⁹.

In the following we will proceed to sketch the kinematical regions affected by NLO corrections and their evaluation. We will not dwell on mistreated regions, which, in a nutshell, require the identification and subtraction of the relevant counterterms in the corresponding points of the NLO calculations.

Large-angle scatterings are not sensitive to soft loop corrections, as they would require internal and/or external soft lines, which are either excluded by construction or suppressed. Hard loops represent an $\mathcal{O}(g^2)$ correction, so that this region is not affected at NLO.

Collinear processes are sensitive to soft loop corrections: they give rise to the $\mathcal{O}(g)$ correction¹² to $\mathcal{C}(x_\perp)$ which we have mentioned in the previous Sections, as well as to an $\mathcal{O}(g)$ correction²⁰ to the dispersion relations of the hard, collinear particles.

Diffusion processes are also naturally sensitive to $\mathcal{O}(g)$ corrections, since the typical momenta there are by construction soft. The soft loop corrections to \hat{q} ¹² have also been mentioned before, while those to \hat{q}_L ¹⁶ will be introduced in the following.

Finally, a new process appears at NLO. We label it *semi-collinear*. It is related to the example we made earlier on in this Section of a large-angle scattering with an incoming (or outgoing) soft gluon, which causes the angle between the two outgoing (or incoming) hard ones to be smaller than in the large-angle case but larger than in the pure collinear case. Indeed, as we shall see, this process will represent a bridge between the other three.

Schematically, the collision operator then takes this form

$$\delta C = \delta C_{\text{coll}} + \delta C_{\text{diff}}[\mu] + \delta C_{\text{semi-coll}}[\mu], \quad (79)$$

where we anticipate, as noted by the μ dependence, that the last two processes will require regulation, but that the dependence on the regulator will vanish in the sum.

5.1. The collinear region

In the collinear regime the $\mathcal{O}(g)$ corrections enter then in two places, as we anticipated: both the effective thermal masses squared m_∞^2 and the collision kernel $\mathcal{C}(x_\perp)$ get $\mathcal{O}(g)$ corrections^r.

For what concerns the thermal masses, an expression in terms of gauge-invariant fermionic and bosonic condensates supported on the light-cone is known.²⁰ It reads^s

$$m_\infty^2 = g^2 C_A Z_g \quad Z_g \equiv \frac{1}{d_A} \left\langle v_\mu F^{\mu\nu a} \left(\frac{1}{(v \cdot D)^2} \right)_{ab} v_\rho F_\nu^{\rho b} \right\rangle, \quad (80)$$

where $v = (1, \mathbf{v})$ is a null vector ($|\mathbf{v}| = 1$). Intuitively, Z_g describes how thermal fluctuations of the gauge fields affect the propagation of a fast, light-like particle.

^r For simplicity we do not illustrate the two further mistreated regions¹⁶ in the soft and semi-collinear limits respectively.

^sIn QCD with quarks there is also a fermionic condensate. Both condensates contribute to the asymptotic masses of gluons and quarks.

It can be rewritten as

$$Z_g = \frac{-1}{d_A} \int_0^\infty dx^+ x^+ \langle v_\mu F_a^{\mu\nu}(x^+) U_A^{ab}(x^+, 0) v_\rho F_b^{\rho\nu}(0) \rangle, \quad (81)$$

which makes the connection with \hat{q} clearer: by comparing with Eq. (29), it is easy to see that they share the same Lorentz structure. At leading order Z_g is dominated by hard ($p \sim T$) momenta and one easily has

$$Z_g^{\text{LO}} = 2 \int \frac{d^3p}{(2\pi)^3 p} n_B(p) = \frac{T^2}{6}. \quad (82)$$

The $\mathcal{O}(g)$ contribution arises from the proper treatment of the IR limit of the above integration, requiring in principle HTL resummation. However, Z_g is supported on a lightcone, so that the methods of Sec. 3 become applicable. As shown by Caron-Huot²⁰ (further details can also be found here¹⁴) the $\mathcal{O}(g)$ contribution is easily obtained from the Euclidean zero-modes, yielding

$$\delta Z_g = T \int \frac{d^3q}{(2\pi)^3} \frac{q_\perp^2}{(q_z + i\epsilon)^2} \left(\frac{-1}{q^2 + m_D^2} + \frac{1}{q^2} \right) = -\frac{Tm_D}{2\pi}, \quad (83)$$

so that the NLO correction to the asymptotic mass δm_∞^2 reads

$$\delta m_\infty^2 = g^2 C_A \left(-\frac{Tm_D}{2\pi} \right). \quad (84)$$

For what concerns the scattering kernel, Caron-Huot¹² has shown that three-body contributions vanish in the three-pole operator sketched below Eq. (43). Hence, also at NLO one just needs the sum of three two-body contributions at different transverse separations. The computation of these is nothing but the NLO contribution to $\mathcal{C}(x_\perp)$. We have shown in detail in Sec. 3.3 how to “Euclideanize” the leading-order calculation. At NLO one then needs to compute one-loop diagrams in three-dimensional EQCD, such as those shown in Fig. 9. The result for



Fig. 9. Two sample diagrams necessary for the NLO evaluation of $\mathcal{C}(q_\perp)$. The conventions are as in Fig. 4.

$\delta \mathcal{C}(q_\perp)$ ¹² and the corresponding $\delta \mathcal{C}(x_\perp)$ ¹⁴ are not shown here for brevity. We point to the references for their expressions. We would like to stress again how the reduction to the Euclidean, three-dimensional theory makes this calculation tremendously simpler. If we were to compute the diagrams of Fig. 9 in the HTL-resummed theory in four Minkowskian dimensions, we would have to deal with complicated

denominators of (up to 4) HTL propagators (see Eq. (54)) and the intricate HTL vertices. Indeed, in both our example diagrams we would need to consider them along the standard bare vertices. In the Euclideanized, three-dimensional theory, on the other hand, the propagators become simple massive or massless ones and the effective vertices just disappear, as they depend linearly on the external frequencies, which vanish in dimensional regularization.^t

In order to obtain the NLO correction to the collinear rate (40), Eq. (43) is then to be perturbed by δm_∞^2 and $\delta \mathcal{C}$. The first order in this perturbation $\delta \mathbf{f}(\mathbf{b})$, is plugged in Eqs. (45) and (40). Details on this procedure may be found in these references.^{14,16} Algorithms for the solution of the differential equation with the correct boundary conditions are discussed in these other works.^{14,15,71,72}

We furthermore stress that, should a factorized approach based on lattice measurements of soft observables, as outlined at the end of Sec. 4, be applied here, one would need a non-perturbative measurement of the aforementioned three-pole operator. It would be interesting to analyze the non-perturbative appearance of three-body forces in such an object.

Finally, we remark that recently it has been pointed out^{73,74} that collinear processes are sensitive to a large, double-logarithmic correction, which also shows up as a double-logarithmic correction to \hat{q} . This term represent a relative $\mathcal{O}(g^2)$ correction in our framework and would hence contribute to NNLO. It would arise from considering the first correction to the eikonal approximation in deriving Eq. (42).

5.2. The diffusion sector at NLO

As we anticipated, the Fokker-Planck diffusion equation (21) still applies. We then need the $\mathcal{O}(g)$ corrections to \hat{q} and \hat{q}_L , which unambiguously determine \hat{e} at NLO through the procedure sketched in Eq. (17). Both can be calculated from their Wilson line definitions (26) and (27). The former is computed with the Euclidean technology of Sec. 3.2 and the latter with the sum rules of Sec. 3.3. However, before going in the details of the two separate calculations, one can proceed to a simplification,^{16,43} which is attained by using the equation of motion of the Wilson line $D_{x^+}^- U(x^+; 0) = 0$ to simplify $F^{-\mu}$ to $\partial^\mu A^-$ (in all gauges but the $A^- = 0$ one) and by noting again that operator ordering is not relevant at NLO: classical soft gluons commute, as we have used in obtaining the simplified forms (29) and (30). The Wilson line structure then simplifies to

$$\hat{q} = \frac{g^2 C_R}{d_A} \int_{-\infty}^{+\infty} dx^+ \langle \partial^\perp A^{-a}(x^+) U_A^{ab}(x^+, 0) \partial^\perp A^{-b}(0) \rangle, \quad (85)$$

$$\hat{q}_L = \frac{g^2 C_R}{d_A} \int_{-\infty}^{+\infty} dx^+ \langle \partial^+ A^{-a}(x^+) U_A^{ab}(x^+, 0) \partial^+ A^{-b}(0) \rangle. \quad (86)$$

Their evaluation requires the computation of the diagrams shown in Fig. 10.

^tIndeed, there are no resummed vertices of the same order of the bare ones in EQCD, as we have shown in Sec. 4.

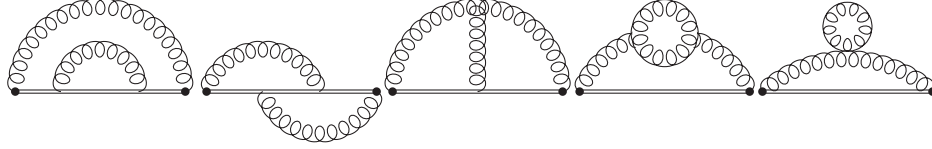


Fig. 10. Diagrams contributing to $\delta\hat{q}$ and $\delta\hat{q}_L$ at NLO. The blobs represent again the field strength insertions. Three- and four-gluon vertices are either bare or resummed HTL vertices.

For what concerns \hat{q} , the reduction to the Euclidean, three-dimensional theory introduced before makes this calculation too tremendously simpler. One then obtains for $\delta\hat{q}$, the NLO contribution to \hat{q} ^{12 u}

$$\delta\hat{q} = \frac{g^4 C_R C_A T^3}{32\pi^2} \frac{m_D}{T} (3\pi^2 + 10 - 4\ln 2). \quad (87)$$

For what concerns $\delta\hat{q}_L$, the sum-rule technology we have introduced in Sec. 3.3 can be applied and leads to another tremendous computational simplification.¹⁶ As a general strategy, we remark that the Wilson line propagators depend only on the minus components of the momenta, so that the plus component, which we call q^+ , can be deformed again. This corresponds to expanding those diagrams for large, complex q^+ . The leading contribution can be of order $(q^+)^0$ and the subleading one of order $(q^+)^{-1}$. Higher-order terms are suppressed and can be neglected. The leading, $\mathcal{O}((q^+)^0)$ term, once integrated along the contour, will give rise to a linear divergence, which has to match with the one arising from the corresponding mistreated region in the collinear process (see footnote r). Indeed, the calculation¹⁶ confirms that the two divergences cancel.

For what concerns the $\mathcal{O}(1/q^+)$ term, we already encountered such behavior at LO, where it gave rise to the asymptotic mass. In the photon case¹⁴ it was found, rather surprisingly, that the NLO contribution to this term amounted to replacing the quark asymptotic mass m_∞^2 with $m_\infty^2 + \delta m_\infty^2$, where δm_∞^2 is its soft $\mathcal{O}(g)$ correction, in the fermionic equivalent of Eq. (71) and then expanding to linear order in δm_∞^2 (and hence in g). The explicit sum-rule computation¹⁶ of the diagrams in Fig. 10 yields the same (up to the different asymptotic mass) i.e.

$$\frac{m_\infty^2 + \delta m_\infty^2}{q_\perp^2 + m_\infty^2 + \delta m_\infty^2} = \frac{m_\infty^2}{q_\perp^2 + m_\infty^2} + \delta m_\infty^2 \frac{q_\perp^2}{(q_\perp^2 + m_\infty^2)^2} + \mathcal{O}(g^2), \quad (88)$$

where δm_∞^2 is given in Eq. (84). This result can be interpreted physically in the following way: expanding for large (complex) q^+ takes the soft fields to approach their collinear limit, where the only effect of resummation is to introduce an asymptotic mass (at leading order) and the soft correction thereto (at next-to-leading order). For this same reason, HTL vertices become small and not relevant.

^uCaron-Huot obtained this result by applying Eq. (36) to his calculation of $\mathcal{C}(q_\perp)$ at NLO. The two methods are completely equivalent, as Eq. (26) can be formally derived from Eqs. (35) and (36) when $\mathcal{C}(q_\perp)$ is defined from the Wilson loop in Fig. 3, as shown in this reference.³³

Hence we obtain

$$\delta\hat{q}_L = g^2 C_R T \int \frac{d^2 q_\perp}{(2\pi)^2} \frac{q_\perp^2 \delta m_\infty^2}{(q_\perp^2 + m_\infty^2)^2} = \frac{g^2 C_R T \delta m_\infty^2}{4\pi} \left[\ln \left(\frac{(\mu^{\text{NLO}})^2}{m_\infty^2} \right) - 1 \right], \quad (89)$$

where we have introduced a regulator μ^{NLO} . As we will show, the semi-collinear region will remove the dependence on it, so that it should be taken to obey $gT \ll \mu^{\text{NLO}} \ll \sqrt{g}T$.

5.3. The semi-collinear region

As we anticipated before, semi-collinear processes can be seen as $1 \leftrightarrow 2$ splitting processes where the opening angle (and hence the virtuality) are larger. Two examples are drawn in Fig. 11. The scalings of this region are as follows: $K \sim gT$ is soft,

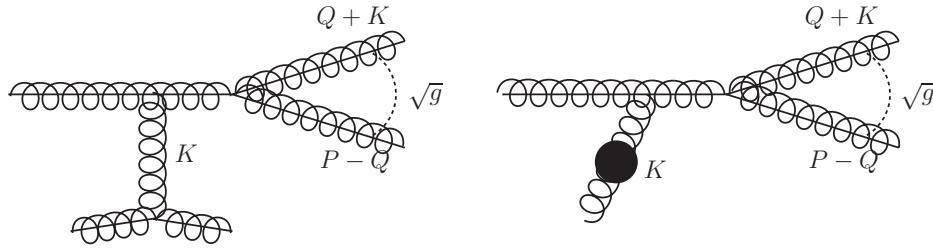


Fig. 11. Diagrams for two typical semi-collinear processes. In the first case the soft gluon is in the spacelike Landau cut, whereas in the second case it is on its timelike plasmon pole, represented by the black blob.

whereas the two final-state particles are collinear, albeit with an increased virtuality and opening angle with respect to the collinear sector. The leading contribution then comes from $q^+ \sim T$, $q^- \sim gT$, $q_\perp^2 \sim gT^2$, $Q^2 \sim gT^2$.

Naive power-counting arguments would suggest that the semi-collinear region should contribute to leading order, as it is the largest slice of phase space where a soft gluon can attach to a $1 \leftrightarrow 2$ process. However, once all diagrams are summed and squared, a cancellation, first noticed in the context of photon radiation,³⁰ introduces an extra $\mathcal{O}(g)$ suppression. Furthermore, since $K \sim gT$ in all components, the contribution from timelike soft gluons, e.g. plasmons, is now allowed. This is contrasted by the collinear region, where kinematics enforce $k^- \sim \delta E \sim g^2 T \ll k^+, k_\perp$, thus restricting soft gluons to the space-like domain only.

The contribution $\delta C_{\text{semi-coll}}$ to the collision operator can be written in the same way as the collinear one, as given by Eq. (42), with the replacement of the collinear

rates with semi-collinear ones. In pure glue it reads¹⁶

$$\delta C_{\text{semi-coll}}[\mu] = \int_{-\infty}^{+\infty} d\omega \left[f_{p+\omega} \frac{d\Gamma(p+\omega, \omega)}{d\omega} \Big|_{\text{semi-coll}} - f_p \theta(p-2\omega) \frac{d\Gamma(p, \omega)}{d\omega} \Big|_{\text{semi-coll}} \right], \quad (90)$$

The derivation of the semi-collinear rates then requires the evaluation of processes of the form of Fig. 11, with $p, q^+ \gg q_\perp \gg k_\perp, k^+$. This results in the following factorized form¹⁶

$$\frac{d\Gamma(p, \omega)}{d\omega} \Big|_{\text{semi-coll}} = \frac{g^2 C_A}{\pi p} \frac{(1-x+x^2)^3}{x(1-x)} (1+n(\omega))(1+n(p-\omega)) \int \frac{d^2 q_\perp}{(2\pi)^2} \frac{\hat{q}(\delta E)}{q_\perp^4} \quad (91)$$

where

$$\delta E = \frac{p q_\perp^2}{2\omega(p-\omega)}, \quad (92)$$

and $\hat{q}(\delta E)$, which was first introduced for photon radiation,¹⁴ is a modified version of \hat{q} which keeps track of the changes in the small light-cone components p^- and q^- , induced by the interaction with the soft degrees of freedom.

In the field-theoretical language of Sec. 2, $\hat{q}(\delta E)$ is given by^v

$$\hat{q}(\delta E) = \frac{g^2 C_R}{d_A} \int_{-\infty}^{\infty} dx^+ e^{ix^+ \delta E} \langle v^\mu F_\mu^{\nu, a}(x^+) U_A^{ab}(x^+, 0) v^\rho F_{\rho\nu}^b(0) \rangle, \quad (93)$$

where we have made use of the simplification discussed in Eq. (85). The dependence on the minus components appears as a simple phase accumulation during the eikonal propagation, so that one can also easily see how Eq. (93) goes into Eq. (26) for $\delta E \rightarrow 0$. Eq. (93) can also be evaluated using Euclidean techniques, yielding¹⁴

$$\hat{q}(\delta E) = g^2 C_R T \int \frac{d^2 k_\perp}{(2\pi)^2} \left[\frac{m_D^2 k_\perp^2}{(k_\perp^2 + \delta E^2)(k_\perp^2 + \delta E^2 + m_D^2)} + \frac{2\delta E^2}{k_\perp^2 + \delta E^2} \right]. \quad (94)$$

As we have anticipated at the beginning of this Section, a counterterm from the large-angle scattering region needs to be subtracted, as well as a collinear one (see footnote r). The former arises from taking the $m_D \rightarrow 0$ limit of Eq. (94) (there is no resummation taking place on external legs at LO) and the latter by taking the $\delta E \rightarrow 0$ limit (changes in the minus component are not accounted for in the collinear

^vStrictly speaking, this is the version that applies to photon radiation and in this case we would need a more complicated three-pole expression, along the lines of the discussion that followed Eq. (43). However, we are evaluating it at the leading-order, one-gluon exchange level, so that the more complicated form is not necessary.

limit). Once these subtractions are performed, the semi-collinear rate becomes

$$\begin{aligned} \left. \frac{d\Gamma(p, \omega)}{d\omega} \right|_{\text{semi-coll}} &= \frac{g^4 C_A^2 T}{\pi p} (1 + n(\omega))(1 + n(p - \omega)) \int \frac{d^2 q_\perp}{(2\pi)^2} \int \frac{d^2 k_\perp}{(2\pi)^2} \frac{1}{q_\perp^4} \\ &\times \frac{(1 - x + x^2)^3}{x(1 - x)} \left[\frac{m_D^2 k_\perp^2}{(k_\perp^2 + \delta E^2)(k_\perp^2 + \delta E^2 + m_D^2)} - \frac{m_D^2}{k_\perp^2 + m_D^2} \right]. \end{aligned} \quad (95)$$

We stress that the semi-collinear collision operator is given by Eq. (90).

The q_\perp integration in Eq. (95) is to be understood as IR-regulated by μ^{NLO} . One can show¹⁶ how the small- ω -and- q_\perp region gives rise to IR logarithms that cancel the μ^{NLO} dependence of diffusion processes. Details of how the transverse integrations can be carried out analytically are also given there. The ω integration remains to be performed numerically.

6. Summary and conclusions

In this review we have shown how at leading and next-to-leading order the propagation, energy loss, and momentum diffusion of high-energy particles in the QGP can be cast in the form of a Boltzmann equation describing the interactions between the jet particles and the hard and soft constituents of the plasma (Eq. (1) and Eq. (79)). In Sec. 2 we introduced this formalism at leading order, where three processes contribute. These processes include $2 \leftrightarrow 2$ scatterings of the jet with the hard particles, drag and (longitudinal and transverse) momentum diffusion induced by the soft highly occupied gluonic background, and collinear bremsstrahlung (and merging) induced by the transverse momentum diffusion. The $2 \leftrightarrow 2$ scatterings are dealt with in a standard kinetic fashion (Eq. (10)), the collinear splittings and joinings give rise to a somewhat simpler rate term (Eq. (42)), and the interactions with the soft background are described by a Fokker-Planck equation (Eq. (21)) or equivalently by a Langevin equation (Eq. (23)).

We have furthermore shown how the contributions of the soft degrees of freedom to the kinetic picture (the diffusion coefficients in the Fokker-Planck equation and the transverse scattering kernel in the collinear rate) can be cleanly defined as correlators of Wilson lines, or Wilson loops, supported on the lightcone or on a light front (see Eqs. (26), (27) and (39)). These Wilson lines are to be evaluated using the Hard Thermal Loop effective theory. We devote Sec. 3 to the illustration of the recent understanding of thermal field theory (including Hard Thermal Loops) on the lightcone. We show how the causal properties of amplitudes at light-like separations bring about a dramatic simplification in their calculation.¹² To put it simply, jet and hard particles, which move at $v \sim c$, probe the medium in a very simple (thermodynamical) way, since the soft background “does not have the time” to respond to the perturbation they cause. At a practical level, we show how the computation of certain lightlike correlators, such as transverse momentum

diffusion, “euclideanizes”, that is, it reduces to a much simpler calculation in the three-dimensional Euclidean theory EQCD (see Eqs. (64) and (65)). We also show how a different set of lightlike correlators, such as longitudinal diffusion, does not euclideanize. This case also simplifies, however, and the same causal properties on the lightcone make it sensitive only to the thermal mass and soft corrections thereto (see Eqs. (70) and (71)).

In Sec. 4 and Sec. 5 we reviewed two major consequences of these lightcone simplifications. First, we showed how operators that euclideanize can be measured on the lattice. Second, we reviewed the consequences on perturbation theory. At leading order the lightcone simplifications result in simple analytical closed forms in place of relatively straightforward numerical integrals. At NLO the impact is much more far-reaching – calculations that would have been extremely intricate, if not impossible, can now be performed with relative ease.

In more detail, in Sec. 4 we reviewed the basics of EQCD, and described the first non-perturbative calculations of \hat{q} and the transverse momentum scattering kernel using this effective theory.¹³ We would like to emphasize how these first results open a new avenue of research – all other Euclidean operators can be measured on the lattice in the same way. This creates the tantalizing possibility of a factorized approach to kinetics, where perturbation theory is used at the hard scale to compute the $2 \leftrightarrow 2$ scatterings and the splitting processes, while the 3D lattice is used at the soft and ultrasoft scales to compute the diffusion processes and the transverse scatterings leading to bremsstrahlung.

In Sec. 5 we give an overview of the NLO generalization of the LO Boltzmann equation. We showed how the three processes at LO are corrected at NLO (see Eq. (79)). Besides the corrections to the LO diffusion and collinear processes, a new *semi-collinear* process enters, which appears as a bridge between the others, being collinear but with relaxed constraints, i.e. going beyond strict collinearity. In the evaluation of each of these processes we sketched how the lightcone simplifications described above make the NLO analysis possible. We described the NLO calculations of transverse¹² and longitudinal¹⁶ momentum diffusion (Eq. (87) and Eq. (89)), and introduced two related Euclidean operators: the condensate Z_g responsible for the thermal mass (Eq. (80)), and $\hat{q}(\delta E)$, a modified version of \hat{q} relevant for the semicollinear bremsstrahlung (Eq. (93)). The corrections to the longitudinal diffusion and drag coefficients at NLO are due to corrections to the thermal mass (or Z_g). Finally, we presented complete expressions for the NLO rates in the Boltzmann equation for pure gauge theory.

The extension of the NLO Boltzmann equation to include light quarks requires one extra process at leading- and next-to-leading order, the *conversion process*, which can be seen as a fermionic analogue of diffusion.¹⁶ The interaction of hard or jet particles with soft quarks results in a conversion from a quark to a gluon with approximately the same momentum and vice-versa. The computation of these rates involve fermionic correlators on the light cone. It turns out that the light-

cone simplifications of the fermionic HTLs are strikingly similar to the longitudinal diffusion described in Sec. 3.3, and consequently the conversion rates are sensitive only to the (fermionic) asymptotic mass and its soft corrections. These corrections to the fermion mass are computable with the 3D effective theory, in much the way that the effective theory can be used to compute corrections to Z_g .

One very important question that we leave to future works is the impact of these developments on calculations of jet energy loss and their comparison to experimental data. We remark that the Monte Carlo event generator MARTINI⁷⁵ currently implements a kinetic approach that is very close to the leading-order picture sketched in Sec. 2. It is then an ideal candidate for the inclusion of the developments discussed in Sec. 4 and Sec. 5. The reorganization in terms of $2 \leftrightarrow 2$ scattering, diffusion and collinear processes, as well as the implementation of the NLO corrections discussed in Sec. 5, is already underway. This can be easily complemented by the inclusion of non-perturbative input. Besides the measured transverse scattering kernel, lattice calculations for $\hat{q}(\delta E)$ and m_∞^2 could easily be included into MARTINI, should they become available in the future. It would also be interesting to see the results of this numerical implementation for the angular structure of jets, for which recent order-of-magnitude estimates from perturbation theory are available.⁷⁶

As a general remark, we find it difficult to tell *a priori* the impact the NLO corrections of Sec. 5 will have. The recent calculation to NLO of the thermal photon rate,¹⁴ (which includes many of the ingredients presented here, such as Euclideanizations, light-cone causality, collinear and semi-collinear processes) showed how the NLO corrections naturally divide into two large, and largely canceling, contributions – see Fig. 12. Clearly the NLO corrections are modest over a significant range of photon momentum. The positive contribution arose from collinear processes enhanced by a NLO increase of the scattering kernel, and a NLO decrease of the thermal mass, while the negative contribution arose from the semi-collinear and NLO soft processes. The large cancellation between these two corrections is largely accidental and is dependent on the details of the medium, such as the number of colors and flavors. Nevertheless, we anticipate a similar cancellation for the current more complicated case of parton energy loss.

Finally, we note that the kinetic approach we have outlined is often used to compute the transport coefficients of QCD plasmas.^{22,77} While an extension to NLO of these calculations requires more than what is outlined in Sec. 5, a computation of transport coefficients in thermal QCD beyond leading order will almost certainly make considerable use of the euclidean light-cone simplifications described in this review.

Acknowledgments

We would like to thank Guy Moore for collaboration in this reference.¹⁶ We also thank Simon Caron-Huot, Aleksi Kurkela, Mikko Laine and Marco Panero for useful

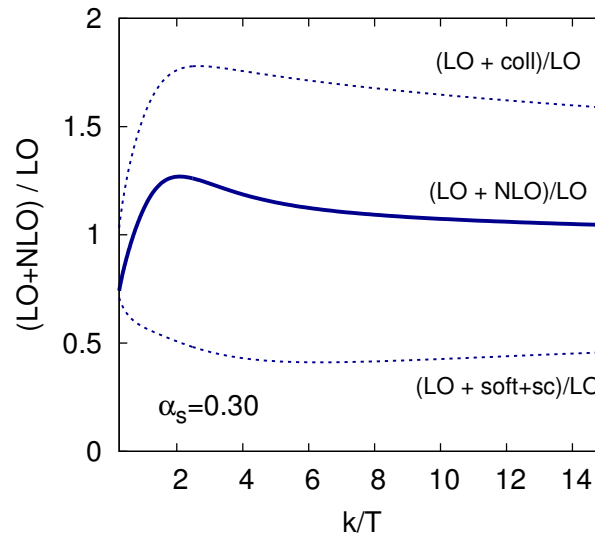


Fig. 12. The differential photon emission rate $d\Gamma_\gamma/dk$ relative to the leading order rate as a function of the photon momentum k/T at a fixed coupling $\alpha_s = 0.3$ in a $N_f = 3$ QGP. The full next-to-leading order rate¹⁴ (LO+NLO) is a sum of the leading order rate (LO), a collinear correction (coll), and a soft+semi-collinear correction (soft+sc). The dashed curve labeled LO+coll shows the ratio of rates when only the collinear correction is included, with the analogous notation for the LO + soft+sc curve. Figure taken from the original reference.¹⁴

conversations. This work was supported in part by the Swiss National Science Foundation (SNF) under grant 200020_155935 and a grant from the U.S. Department of Energy, DE-FG-02-08ER4154.

References

1. G. Roland, K. Safarik, and P. Steinberg, Heavy-ion collisions at the LHC, *Prog.Part.Nucl.Phys.* **77**, 70–127, (2014). doi: 10.1016/j.pnpnp.2014.05.001.
2. D. d’Enterria, Jet quenching, *Springer Verlag, Landholt-Boernstein*. **Vol. 1-23A**, (2009).
3. A. Majumder and M. Van Leeuwen, The Theory and Phenomenology of Perturbative QCD Based Jet Quenching, *Prog.Part.Nucl.Phys.* **A66**, 41–92, (2011). doi: 10.1016/j.pnpnp.2010.09.001.
4. Y. Mehtar-Tani, J. G. Milhano, and K. Tywoniuk, Jet physics in heavy-ion collisions, *Int.J.Mod.Phys.* **A28**, 1340013, (2013). doi: 10.1142/S0217751X13400137.
5. R. Baier, D. Schiff, and B. Zakharov, Energy loss in perturbative QCD, *Ann.Rev.Nucl.Part.Sci.* **50**, 37–69, (2000). doi: 10.1146/annurev.nucl.50.1.37.
6. G. Qin and X.-N. Wang, Jet quenching in heavy-ion collisions, *this volume*. (2015).
7. J.-P. Blaizot and Y. Mehtar-Tani, Color decoherence and jet structure inside the QGP, *this volume*. (2015).
8. E. Braaten and R. D. Pisarski, Soft Amplitudes in Hot Gauge Theories: A General Analysis, *Nucl.Phys.* **B337**, 569, (1990). doi: 10.1016/0550-3213(90)90508-B.

9. E. Braaten and R. D. Pisarski, Simple effective Lagrangian for hard thermal loops, *Phys. Rev.* **D45**, 1827–1830, (1992). doi: 10.1103/PhysRevD.45.R1827.
10. J.-P. Blaizot and E. Iancu, The Quark gluon plasma: Collective dynamics and hard thermal loops, *Phys.Rept.* **359**, 355–528, (2002). doi: 10.1016/S0370-1573(01)00061-8.
11. P. B. Arnold, G. D. Moore, and L. G. Yaffe, Effective kinetic theory for high temperature gauge theories, *JHEP.* **0301**, 030, (2003). doi: 10.1088/1126-6708/2003/01/030.
12. S. Caron-Huot, O(g) plasma effects in jet quenching, *Phys.Rev.* **D79**, 065039, (2009). doi: 10.1103/PhysRevD.79.065039.
13. M. Panero, K. Rummukainen, and A. Schäfer, A lattice study of the jet quenching parameter, *Phys.Rev.Lett.* **112**, 162001, (2014). doi: 10.1103/PhysRevLett.112.162001.
14. J. Ghiglieri, J. Hong, A. Kurkela, E. Lu, G. D. Moore, and D. Teaney, Next-to-leading order thermal photon production in a weakly coupled quark-gluon plasma, *JHEP.* **1305**, 010, (2013). doi: 10.1007/JHEP05(2013)010.
15. J. Ghiglieri and G. D. Moore, Low Mass Thermal Dilepton Production at NLO in a Weakly Coupled Quark-Gluon Plasma, *JHEP.* **1412**, 29, (2014). doi: 10.1007/JHEP12(2014)029.
16. J. Ghiglieri, G. D. Moore, and D. Teaney, Evolution of leading partons at NLO, *in preparation.* (2015).
17. O. K. Kalashnikov and V. V. Klimov, Polarization Tensor in QCD for Finite Temperature and Density, *Sov. J. Nucl. Phys.* **31**, 699, (1980).
18. H. A. Weldon, Covariant Calculations at Finite Temperature: The Relativistic Plasma, *Phys. Rev.* **D26**, 1394, (1982).
19. J.-P. Blaizot, A. Ipp, A. Rebhan, and U. Reinosa, Asymptotic thermal quark masses and the entropy of QCD in the large- $N(f)$ limit, *Phys.Rev.* **D72**, 125005, (2005). doi: 10.1103/PhysRevD.72.125005.
20. S. Caron-Huot, On supersymmetry at finite temperature, *Phys.Rev.* **D79**, 125002, (2009). doi: 10.1103/PhysRevD.79.125002.
21. B. Svetitsky, Diffusion of charmed quarks in the quark-gluon plasma, *Phys.Rev.* **D37**, 2484–2491, (1988). doi: 10.1103/PhysRevD.37.2484.
22. P. B. Arnold, G. D. Moore, and L. G. Yaffe, Transport coefficients in high temperature gauge theories. 1. Leading log results, *JHEP.* **0011**, 001, (2000). doi: 10.1088/1126-6708/2000/11/001.
23. J. Hong and D. Teaney, Spectral densities for hot QCD plasmas in a leading log approximation, *Phys.Rev.* **C82**, 044908, (2010). doi: 10.1103/PhysRevC.82.044908.
24. P. B. Arnold, Langevin equations with multiplicative noise: Resolution of time discretization ambiguities for equilibrium systems, *Phys.Rev.* **E61**, 6091–6098, (2000). doi: 10.1103/PhysRevE.61.6091.
25. P. B. Arnold, Symmetric path integrals for stochastic equations with multiplicative noise, *Phys.Rev.* **E61**, 6099–6102, (2000). doi: 10.1103/PhysRevE.61.6099.
26. P. B. Arnold and W. Xiao, High-energy jet quenching in weakly-coupled quark-gluon plasmas, *Phys.Rev.* **D78**, 125008, (2008). doi: 10.1103/PhysRevD.78.125008.
27. C. Kittel, *Elementary Statistical Physics*. Dover Books on Physics Series, (Dover Publications, 2004). ISBN 9780486435145.
28. P. B. Arnold, Simple Formula for High-Energy Gluon Bremsstrahlung in a Finite, Expanding Medium, *Phys.Rev.* **D79**, 065025, (2009). doi: 10.1103/PhysRevD.79.065025.
29. R. Baier, A. H. Mueller, D. Schiff, and D. Son, 'Bottom up' thermalization in heavy ion collisions, *Phys.Lett.* **B502**, 51–58, (2001). doi: 10.1016/S0370-2693(01)00191-5.
30. P. B. Arnold, G. D. Moore, and L. G. Yaffe, Photon emission from ultrarelativistic plasmas, *JHEP.* **0111**, 057, (2001).
31. P. B. Arnold, G. D. Moore, and L. G. Yaffe, Photon and gluon emission in relativistic

- plasmas, *JHEP*. **0206**, 030, (2002).
32. F. D'Eramo, H. Liu, and K. Rajagopal, Transverse Momentum Broadening and the Jet Quenching Parameter, Redux, *Phys.Rev.* **D84**, 065015, (2011). doi: 10.1103/PhysRevD.84.065015.
 33. M. Benzke, N. Brambilla, M. A. Escobedo, and A. Vairo, Gauge invariant definition of the jet quenching parameter, *JHEP*. **1302**, 129, (2013). doi: 10.1007/JHEP02(2013)129.
 34. S. Jeon and G. D. Moore, Energy loss of leading partons in a thermal QCD medium, *Phys.Rev.* **C71**, 034901, (2005). doi: 10.1103/PhysRevC.71.034901.
 35. R. Baier, Y. L. Dokshitzer, S. Peigne, and D. Schiff, Induced gluon radiation in a QCD medium, *Phys.Lett.* **B345**, 277–286, (1995). doi: 10.1016/0370-2693(94)01617-L.
 36. R. Baier, Y. L. Dokshitzer, A. H. Mueller, S. Peigne, and D. Schiff, Radiative energy loss of high-energy quarks and gluons in a finite volume quark - gluon plasma, *Nucl.Phys.* **B483**, 291–320, (1997). doi: 10.1016/S0550-3213(96)00553-6.
 37. B. Zakharov, Fully quantum treatment of the Landau-Pomeranchuk-Migdal effect in QED and QCD, *JETP Lett.* **63**, 952–957, (1996). doi: 10.1134/1.567126.
 38. B. Zakharov, Radiative energy loss of high-energy quarks in finite size nuclear matter and quark - gluon plasma, *JETP Lett.* **65**, 615–620, (1997). doi: 10.1134/1.567389.
 39. P. B. Arnold, D. T. Son, and L. G. Yaffe, Effective dynamics of hot, soft nonAbelian gauge fields. Color conductivity and $\log(1/\alpha)$ effects, *Phys.Rev.* **D59**, 105020, (1999). doi: 10.1103/PhysRevD.59.105020.
 40. D. F. Litim and C. Manuel, Semiclassical transport theory for nonAbelian plasmas, *Phys.Rept.* **364**, 451–539, (2002). doi: 10.1016/S0370-1573(02)00015-7.
 41. S. Caron-Huot, Hard thermal loops in the real-time formalism, *JHEP*. **0904**, 004, (2009). doi: 10.1088/1126-6708/2009/04/004.
 42. E. Braaten, R. D. Pisarski, and T.-C. Yuan, Production of Soft Dileptons in the Quark - Gluon Plasma, *Phys.Rev.Lett.* **64**, 2242, (1990). doi: 10.1103/PhysRevLett.64.2242.
 43. S. Caron-Huot and G. D. Moore, Heavy quark diffusion in QCD and $N=4$ SYM at next-to-leading order, *JHEP*. **0802**, 081, (2008). doi: 10.1088/1126-6708/2008/02/081.
 44. P. B. Arnold, G. D. Moore, and L. G. Yaffe, Photon emission from quark gluon plasma: Complete leading order results, *JHEP*. **0112**, 009, (2001).
 45. V. Alves, A. K. Das, and S. Perez, Light front field theories at finite temperature, *Phys.Rev.* **D66**, 125008, (2002). doi: 10.1103/PhysRevD.66.125008.
 46. H. A. Weldon, Thermal selfenergies using light front quantization, *Phys.Rev.* **D67**, 128701, (2003). doi: 10.1103/PhysRevD.67.128701.
 47. H. A. Weldon, Thermal selfenergies using light front quantization, *Phys.Rev.* **D67**, 128701, (2003). doi: 10.1103/PhysRevD.67.128701.
 48. P. Aurenche, F. Gelis, and H. Zaraket, A Simple sum rule for the thermal gluon spectral function and applications, *JHEP*. **0205**, 043, (2002).
 49. E. Braaten and M. H. Thoma, Energy loss of a heavy fermion in a hot plasma, *Phys.Rev.* **D44**, 1298–1310, (1991). doi: 10.1103/PhysRevD.44.1298.
 50. D. Besak and D. Bödeker, Thermal production of ultrarelativistic right-handed neutrinos: Complete leading-order results, *JCAP*. **1203**, 029, (2012). doi: 10.1088/1475-7516/2012/03/029.
 51. S. Peigne and A. Peshier, Collisional Energy Loss of a Fast Muon in a Hot QED Plasma, *Phys.Rev.* **D77**, 014015, (2008). doi: 10.1103/PhysRevD.77.014015.
 52. M. Laine and A. Rothkopf, Light-cone Wilson loop in classical lattice gauge theory, *JHEP*. **1307**, 082, (2013). doi: 10.1007/JHEP07(2013)082.
 53. A. Majumder, Calculating the jet quenching parameter q in lattice gauge theory,

- Phys.Rev.* **C87**, 034905, (2013). doi: 10.1103/PhysRevC.87.034905.
54. E. Braaten, Solution to the perturbative infrared catastrophe of hot gauge theories, *Phys.Rev.Lett.* **74**, 2164–2167, (1995). doi: 10.1103/PhysRevLett.74.2164.
 55. E. Braaten and A. Nieto, Effective field theory approach to high temperature thermodynamics, *Phys.Rev.* **D51**, 6990–7006, (1995). doi: 10.1103/PhysRevD.51.6990.
 56. E. Braaten and A. Nieto, Free energy of QCD at high temperature, *Phys.Rev.* **D53**, 3421–3437, (1996). doi: 10.1103/PhysRevD.53.3421.
 57. K. Kajantie, M. Laine, K. Rummukainen, and M. E. Shaposhnikov, Generic rules for high temperature dimensional reduction and their application to the standard model, *Nucl.Phys.* **B458**, 90–136, (1996). doi: 10.1016/0550-3213(95)00549-8.
 58. K. Kajantie, M. Laine, K. Rummukainen, and M. E. Shaposhnikov, 3-D SU(N) + adjoint Higgs theory and finite temperature QCD, *Nucl.Phys.* **B503**, 357–384, (1997). doi: 10.1016/S0550-3213(97)00425-2.
 59. A. D. Linde, Infrared Problem in Thermodynamics of the Yang-Mills Gas, *Phys.Lett.* **B96**, 289, (1980). doi: 10.1016/0370-2693(80)90769-8.
 60. A. Hietanen, K. Kajantie, M. Laine, K. Rummukainen, and Y. Schroder, Three-dimensional physics and the pressure of hot QCD, *Phys.Rev.* **D79**, 045018, (2009). doi: 10.1103/PhysRevD.79.045018.
 61. M. Laine, Electroweak phase transition beyond the standard model, *Strong and Electroweak Matter 2000 proceedings*. pp. 58–69, (2000).
 62. M. Laine, G. Nardini, and K. Rummukainen, Lattice study of an electroweak phase transition at $m_h \sim 126$ GeV, *JCAP*. **1301**, 011, (2013). doi: 10.1088/1475-7516/2013/01/011.
 63. M. Laine and O. Philipsen, The Nonperturbative QCD Debye mass from a Wilson line operator, *Phys.Lett.* **B459**, 259–264, (1999). doi: 10.1016/S0370-2693(99)00641-3.
 64. M. Laine, A non-perturbative contribution to jet quenching, *Eur.Phys.J.* **C72**, 2233, (2012). doi: 10.1140/epjc/s10052-012-2233-5.
 65. K. Kajantie, M. Laine, K. Rummukainen, and Y. Schröder, The Pressure of hot QCD up to $g_6 \ln(1/g)$, *Phys.Rev.* **D67**, 105008, (2003). doi: 10.1103/PhysRevD.67.105008.
 66. M. Laine and Y. Schroder, Two-loop QCD gauge coupling at high temperatures, *JHEP*. **0503**, 067, (2005). doi: 10.1088/1126-6708/2005/03/067.
 67. S. Borsanyi, G. Endrodi, Z. Fodor, S. Katz, and K. Szabo, Precision SU(3) lattice thermodynamics for a large temperature range, *JHEP*. **1207**, 056, (2012). doi: 10.1007/JHEP07(2012)056.
 68. M. D’Onofrio, A. Kurkela, and G. D. Moore, Renormalization of Null Wilson Lines in EQCD, *JHEP*. **1403**, 125, (2014). doi: 10.1007/JHEP03(2014)125.
 69. J. Casalderrey-Solana, D. C. Gulhan, J. G. Milhano, D. Pablos, and K. Rajagopal, A Hybrid Strong/Weak Coupling Approach to Jet Quenching, *JHEP*. **1410**, 19, (2014). doi: 10.1007/JHEP10(2014)019.
 70. B. Brandt, A. Francis, M. Laine, and H. Meyer, A relation between screening masses and real-time rates, *JHEP*. **1405**, 117, (2014). doi: 10.1007/JHEP05(2014)117.
 71. P. Aurenche, F. Gelis, G. Moore, and H. Zaraket, Landau-Pomeranchuk-Migdal resummation for dilepton production, *JHEP*. **0212**, 006, (2002).
 72. I. Ghisoiu and M. Laine, Interpolation of hard and soft dilepton rates, *JHEP*. **1410**, 83, (2014). doi: 10.1007/JHEP10(2014)083.
 73. T. Liou, A. Mueller, and B. Wu, Radiative p_\perp -broadening of high-energy quarks and gluons in QCD matter, *Nucl.Phys.* **A916**, 102–125, (2013). doi: 10.1016/j.nuclphysa.2013.08.005.
 74. J.-P. Blaizot, F. Dominguez, E. Iancu, and Y. Mehtar-Tani, Probabilistic picture for medium-induced jet evolution, *JHEP*. **1406**, 075, (2014). doi: 10.1007/JHEP06(2014)

- 075.
- 75. B. Schenke, C. Gale, and S. Jeon, MARTINI: An Event generator for relativistic heavy-ion collisions, *Phys.Rev.* **C80**, 054913, (2009). doi: 10.1103/PhysRevC.80.054913.
 - 76. A. Kurkela and U. A. Wiedemann, Picturing perturbative parton cascades in QCD matter, *Phys.Lett.* **B740**, 172–178, (2014). doi: 10.1016/j.physletb.2014.11.054.
 - 77. P. B. Arnold, G. D. Moore, and L. G. Yaffe, Transport coefficients in high temperature gauge theories. 2. Beyond leading log, *JHEP.* **0305**, 051, (2003). doi: 10.1088/1126-6708/2003/05/051.